

AperTO - Archivio Istituzionale Open Access dell'Università di Torino

Long-term eruptive trends from space-based thermal and SO₂ emissions: a comparative analysis of Stromboli, Batu Tara and Tinakula volcanoes

This is a pre print version of the following article:

Original Citation:

Availability:

This version is available <http://hdl.handle.net/2318/1684782> since 2018-12-18T14:33:33Z

Published version:

DOI:10.1007/s00445-018-1242-0

Terms of use:

Open Access

Anyone can freely access the full text of works made available as "Open Access". Works made available under a Creative Commons license can be used according to the terms and conditions of said license. Use of all other works requires consent of the right holder (author or publisher) if not exempted from copyright protection by the applicable law.

(Article begins on next page)

See discussions, stats, and author profiles for this publication at: <https://www.researchgate.net/publication/326959591>

Long-term eruptive trends from space-based thermal and SO₂ emissions: a comparative analysis of Stromboli, Batu Tara and Tinakula volcanoes

Article in *Bulletin of Volcanology* · September 2018

DOI: 10.1007/s00445-018-1242-0

CITATIONS

0

READS

115

5 authors, including:



Marco Laiolo

University of Florence; Univeristy of Turin

48 PUBLICATIONS 480 CITATIONS

[SEE PROFILE](#)



Francesco Massimetti

Università degli Studi di Torino

7 PUBLICATIONS 3 CITATIONS

[SEE PROFILE](#)



Corrado Cigolini

Università degli Studi di Torino

80 PUBLICATIONS 914 CITATIONS

[SEE PROFILE](#)



Maurizio Ripepe

University of Florence

264 PUBLICATIONS 5,512 CITATIONS

[SEE PROFILE](#)

Some of the authors of this publication are also working on these related projects:



Secondary Metabolites, Human Homeostasis and Health [View project](#)



Multidisciplinary approach of geothermal prospection in the Argentera Massif (South-Western Alps) [View project](#)

**Long-term eruptive trends from space-based thermal and SO₂ emissions:
a comparative analysis of Stromboli, Batu Tara and Tinakula volcanoes**

Laiolo, M.^{1,2}; Massimetti, F.¹; Cigolini, C.²; Ripepe, M.¹ & Coppola, D.²

1 – Dipartimento di Scienze della Terra, Università di Firenze, V. G. La Pira 4, 50121 Firenze

2 – Dipartimento di Scienze della Terra, Università di Torino, Via Valperga Caluso 35, 10125
Torino

Corresponding Author: Marco Laiolo

Email address: marco.laiolo@unito.it

ORCID-ID: 14013461100

Keywords

Stromboli twins; MODIS; OMI; Volcanic Radiative Power; gas/magma balance; magma budget

Abstract

Batu Tara (Indonesia) and Tinakula (Solomon Island) are two poorly known volcanoes with morphologies and short-term eruptive activity similar to Stromboli (Italy). However, quantitative information about their long-term eruptive behaviours are limited, making the comparisons with Stromboli descriptive and based on short periods of observations. Here, we use over a decade of satellite data to measure and compare the radiant flux (2000–2017) and the SO₂ mass (2004–2017) of all three volcanoes. The combined analysis of Volcanic Radiant Power (from MODIS data) and SO₂ flux (from OMI data) reveals different long-term eruptive trends and contrasting ratios of SO₂/VRP. These data indicate that the eruptive mechanisms operating at each volcano are quite different. The persistent open-vent activity of Stromboli volcano is episodically interrupted by flank eruptions that drain degassed magma stored in the very shallow portion of the central conduit. In contrast, a long-lasting exponential decay of both VRP and SO₂ flux observed at Batu Tara is consistent with the eruption of undegassed magma from a deep, closed magma chamber. Finally, Tinakula displays multiple year-long eruptive phases, characterised by evolving gas/thermal ratios and an eruptive intensity increasing with time. Magma budget calculations for this volcano are consistent with eruption from a volatile-zoned magma chamber, coupled with periods of gas/magma accumulations at depth. Our results suggest that the combined analysis of satellite thermal/gas data is a valuable tool for decrypting the long-term volcanic dynamics that could remain hidden over shorter time-scales.

Introduction

Satellite instruments represent an invaluable resource for measuring eruptive activity at remote volcanoes. In particular, they are unique in providing three main types of datasets, namely: thermal (radiant) flux (e.g. Ramsey and Harris 2013; Wright et al., 2015; Coppola et al. 2016a), gas (SO₂) flux (e.g. Fioletov et al. 2016; Flower et al. 2016; Carn et al. 2017), and deformation (e.g. Biggs et al. 2014; McCormick-Kilbride et al. 2016; Biggs and Pritchard 2017). Data collected from space provide safe, continuous and homogeneous datasets to enable long-term observations of global volcanic activity and detection of volcanic unrest at poorly-monitored volcanoes (e.g. Wright et al. 2005; Chaussard et al. 2013; Coppola et al. 2015). While satellite data are becoming an essential input for real-time volcano hazard assessment (e.g. Ganci et al. 2012; Pyle et al. 2013; Harris et al. 2017), their back-analysis also permits the recognition of eruptive trends and patterns otherwise impossible at volcanoes lacking a ground-based monitoring network (e.g. Coppola et al. 2017a; Dean et al. 1998; Flower et al. 2016). Moreover, the growing databases of remote sensed data allows reconstruction emission of deformation histories, essentially at each volcano on earth, and permit a direct comparison between different volcanoes, both at local and global scales (cf. Harris 2013; Wright et al. 2015; Biggs and Pritchard 2017; Carn et al. 2017).

Batu Tara (7.792°S, 123.579°E) and Tinakula (10.38°S, 165.8°E) are two remote, unmonitored, active volcanoes located in the Lesser Sunda archipelago (Indonesia) and Solomon Islands, respectively (Fig. 1). They have a remarkable resemblance to the well-studied Stromboli (38.789°N, 15.213°E) volcano (Italy), a feature that has earned them the titles of "Stromboli of the Banda Sea", or "Stromboli of the Solomon Islands", or more generally "Stromboli twins" (Batu Tara and Tinakula Global Volcanism Program main pages, <https://volcano.si.edu/volcano.cfm?vn=264260>, <https://volcano.si.edu/volcano.cfm?vn=256010>).

This similarity derives from the evident morpho-structural similarity of the islands (Fig. 2), as well as from the rare field observations (Gaudin et al. 2017) and reports (Rothery et al. 2005) that describe their main activity as “strombolian” (that is characterised by persistent degassing and intermittent mild explosions; see Barberi et al. 1993).

However, the absence of in-situ monitoring instruments, as well as the difficulties of reaching and landing on the islands, make measurements sporadic, with only very few studies focused on the description and characterisation of their eruptive activity (Rothery et al. 2005; Gaudin et al. 2017). Consequently, Tinakula and Batu Tara volcanoes have had low scientific coverage (one and seven papers, respectively) compared to Stromboli whose evolution, structure and eruptive dynamic is much more studied (more than 800 papers based on Scopus database since 1980, <https://www.scopus.com>). It is thus clear that a rigorous and long-term analysis of the eruptive activity characterising Batu Tara and Tinakula is still lacking, making the comparison with Stromboli purely descriptive and based exclusively on short-term behaviours (i.e., on the scale of single explosive event(s); Gaudin et al. 2017).

In this paper we characterise, the long-term thermal and degassing activity (2000–2017) of Batu Tara, Tinakula and Stromboli volcanoes by using satellite data acquired by three different sensors. To track and quantify the radiant heat flux, in terms of Volcanic Radiative Power (VRP in Watt), at each volcano, we used the Moderate Resolution Imaging Spectroradiometer (MODIS) data. The location and extension of the thermal anomalies have been constrained by using thermal images collected by the Advanced Spaceborne Thermal Emission and Reflection Radiometer (ASTER). Data acquired by the Ozone Measurement Instrument (OMI) were used to estimate the daily SO₂ flux (ϕ SO₂ in Tonnes/day) associated with the volcanic gas emissions. Whilst for Batu Tara, Tinakula volcanoes these space-based data sets represent a unique source of information, here we

used Stromboli volcano as a benchmark for satellite data, because of the substantial understanding of its plumbing system and eruptive mechanisms (e.g. Allard et al. 1994; Aiuppa et al. 2010; Métrich et al. 2009; Ripepe et al. 2008, 2015).

Previous works successfully adopted similar combinations of thermal and degassing measurements, to provide insight into the geometry of the plumbing systems and investigate the balance between exogenous versus endogenous growth (e.g. Harris and Stevenson 1997; Steffke et al. 2011; Koeppen et al. 2011; Barrière et al. 2017; Coppola et al. 2016b; 2017a; Aiuppa et al. 2018). In fact, the radiant flux sourced by effusive activity can be used to constrain the lava discharge rate (e.g. Harris et al. 1998; Harris et al. 2007; Coppola et al., 2013), as well as to infer the rate at which the magma circulate at superficial levels, at open-vent volcanoes (e.g. Francis et al. 1993; Oppenheimer et al. 2004; Aiuppa et al. 2018). At the same time, the SO₂ flux from a volcanic vent is widely used to determine the rate at which magma is supplied to shallow levels and degas (e.g. Allard et al. 1994; Francis et al. 1993; Andres and Kasgnoc 1998; Shinohara 2008). Hence, coeval thermal and gas measurements can be used to investigate the magma-gas differentiation processes and to address the occurrence of the so called “excess degassing” (i.e. degassing of unerupted magma with a much larger volume than that of erupted magma), one of the most important concepts in understanding the volatile budget, eruption mechanisms, and differentiation of magmas in the crust (e.g. Allard et al. 1994; Andres and Kasgnoc 1998; Francis et al. 1993; Shinohara 2008).

In the following sections, we firstly describe the main tectonic, geochemical and morphological features of the three volcanoes by outlining similarities and differences from previous works and observations. Then, we present the analysis of 17-year-long records of satellite data acquired over the three volcanoes, in order to: (i) evaluate the persistence and intensity of the volcanic emissions

(thermal and gas), (ii) identify long-term changes in the eruptive behaviours; (iii) evaluate the partitioning between erupted and degassed magma by focussing on the $\phi\text{SO}_2/\text{VRP}$ ratio.

Despite the qualitative resemblance, our results outline marked differences in the eruptive mechanisms of the three volcanoes, which suggest quite different architectures and development of their respective plumbing systems.

Stromboli, Batu Tara and Tinakula volcanoes

The principal features of the three analysed volcanoes, retrieved from the available literature, are summarised in Table 1. Here, we briefly describe their main similarities and differences based on four main aspects: (i) tectonic setting and geochemistry, (ii) morphology, (iii) eruptive products, and (iv) volcanic activity.

Tectonic setting, morphology and erupted products

The tectonic setting of all three volcanoes is consistent with subduction-related magmatism, variably contaminated by slab-derived fluids and/or crustal materials (Elburg et al. 2004; Schuth et al. 2009) and likely overprinted by rift-type processes (De Astis et al. 2003). Recent erupted products (see Table 1) span High-K calc-alkaline basalts for Stromboli (Landi et al. 2009) to potassic-ultrapotassic tephrites for Batu Tara (Van Bergen et al. 1992) and low-potassic (tholeiitic) basalts for Tinakula (Schuth et al. 2009).

All the three islands represent the emerged parts of volcanic edifices rising approximately 3 to 4 km above their respective abyssal plains (Table 1). The sub-aerial volcanic cones are characterised by similar volumes (from 1.3 to 3.9 km³), elevations (from 748 to 924 m above sea level) and mean slopes of volcanic flanks (from 22° to 25°). All the three volcanic edifices are truncated by

a horse-shoe shape scar, resulting from major lateral collapses, termed here a *Sciara del Fuoco*-type collapse following the local name for the collapse scar on Stromboli (Kokelaar and Romagnoli 1995; Tibaldi 2001). The scars host most of the recent volcanic products, erupted from one or more craters located in their higher portions (Fig. 2). Erupted products at the three volcanoes include lava flows, typical of effusive activity, as well as scoria, bombs and ash, typical of mild to moderate explosive activity (Table 1).

Recent activity

Stromboli is known for its persistent activity over 2 ka (Rosi et al. 2000), characterised by continuous degassing at summit vents with scoria, bombs, lapilli and ash ejection that normally occur every 15–20 minutes (Newhall and Self 1982, Barberi et al. 1993; Rosi et al. 2000). Periodically, flank effusive episodes interrupt the explosive summit activity, as observed on 2002–2003, 2007 and 2014 (Ripepe et al. 2017). Paroxysmal explosions may occasionally occur (e.g., 5 April 2003 and 15 March 2007) resulting from rapid decompression of the plumbing system during effusive eruptions (Calvari et al. 2011; Valade et al. 2016). Volcanogenic tsunamis, which affect the Stromboli coastline, have been also observed and are associated to the opening of lateral eruptive fissures triggering flank failure and collapses (Barberi et al. 1993).

The first historical observations of Batu Tara activity describe continuous effusive activity between 1847–1852 (GVP 2007). Subsequently, the volcano entered in a 155-year period of quiescence until January 2007, when a new eruption began (GVP 2007). According to periodic reports, between 2007 and 2011, an effusive activity was accompanied with strombolian to vulcanian explosions, producing ash-rich plumes that reached altitudes of 2–4 km (GVP 2007, 2011, 2014). During 2014, Batu Tara eruptions were characterised by a low-level explosive

activity dominated by gas-poor and ash-rich emissions (Gaudin et al. 2017). Notably, no further ash plumes and thermal anomalies were reported after October 2016 (GVP 2016). Eruptions of Tinakula volcano have been regularly reported since at least 1768 (<https://volcano.si.edu/volcano.cfm?vn=256010>). The eruptive phases typically last months to years and are often separated by periods of repose lasting years to decades (GVP 2003; Rothery et al. 2005). The 1971 eruptive episode (one of the major eruptions of Tinakula in historical time) was characterised by lava flows and ash-dominated explosive activity, which caused a tsunami that led to the evacuation of the island (GVP 1971). Recent observations suggest the occurrence of strombolian activity at the active summit crater(s), accompanied by glowing ejecta often rolling down the steep slope of the scar (Cook et al. 2012). This mild explosive activity is generally characterised by a Volcanic Explosivity Index (VEI; Newhall and Self 1982) of between 1 and 2, with volcanic plume heights not exceeding 4 km in altitude (Database Eruption search curated by the Smithsonian Institution Global Volcanism Program; http://volcano.si.edu/search_eruption.cfm). Notably, on 21 October 2017, a short and intense eruptive phase produced an ash and gas plume reaching an altitude of about 10.7 km above sea level. This unexpected eruption was classified as a VEI 3 explosion (NDMO Report 2017) and represents a major event in the eruptive history of this volcano.

Methods

Here we briefly summarise the methods and analytical procedures used to retrieve the radiant heat flux (VRP), the SO₂ flux (ϕ SO₂), and to spatially characterise the thermal anomalies observed at the three volcanoes.

Volcanic Radiative Power (VRP) via MODIS-MIROVA data

In order to quantify the Volcanic Radiative Power (VRP in Watt) at the three volcanoes we used nighttime data acquires between 2000 and 2017 by the two MODIS instruments. MODIS is a multispectral imager mounted on board of Terra and Aqua NASA's satellites, launched on February 2000 and May 2002, respectively. We used the MODIS Level 1B data (1 km² of resolution in the infrared bands) provided by LANCE-MODIS system (<http://lance-modis.eosdis.nasa.gov/>) and elaborated by the MIROVA system (<http://www.mirovaweb.it/>; Coppola et al. 2016c). MIROVA is an automatic hot spot detection system based on the analysis of Middle InfraRed (MIR) radiation detected by MODIS at ~4 μm (channels 21 and 22; see Coppola et al. 2016c). Hence, for any alerted pixel, the VRP is calculated by using the MIR-method proposed by Wooster and coauthors (2003):

$$VRP_{PIX} = 18.9 \times A_{PIX} \times (L_{4alert} - L_{4bk}) \quad (1)$$

where A_{PIX} , L_{4alert} and L_{4bk} are the pixel area (1 km² for MODIS), and the spectral radiance at 4 μm for the alerted pixel(s) and local background, respectively. When two or more pixels (a cluster of pixels) are detected, the total radiative power is calculated as the sum of each single VRP_{PIX} . According to Wooster and coauthors (2003) the MIR-method provides reliable estimates of radiant power ($\pm 30\%$) for hot targets that have an integrated temperature comprised between 600 and 1500 K. It follows that the VRP is appropriate to calculate the heat radiated by the active portions of lava flows, or any other volcanic emitters having a temperature higher than ~300 °C. Errors and limits associated to the MODIS-MIROVA data are described in the Online Resource 1.

The frequency distribution of VRP recorded at the three investigated volcanoes between 2000–2017 has been also analysed in order to detect and eventually discriminate thermal regimes associated to distinct types of volcanic activity (Coppola et al. 2012; Coppola and Cigolini 2013).

Location and extension of thermal anomaly using ASTER

The ASTER instrument, on board of Terra's satellite, provides radiance measurements in 14 spectral bands, spanning from visible and near infrared (VNIR channels 1 to 3b) , short-wave infrared (SWIR channels 4 to 9) and thermal infrared (TIR channels 10 to 13) wavelengths, with spatial resolutions of 15, 30 and 90 m, respectively (Pieri and Abrams 2004). Since 2008, the SWIR images ceased to be available due to a cooling system malfunction (Ramsey 2016).

Unlike MODIS, the acquisition of ASTER images is a scheduled in response to individual acquisition requests, or in emergency response to natural disasters, with a complex scheduling and processing plan based on a scale of priorities (i.e. Expedited Data System EDS; Ramsey 2016). Consequently, ASTER does not necessarily provide systematic observations at all volcanoes, but can be used as a valuable complement to the MODIS (Vaughan et al. 2012; Murphy et al. 2013) or other moderate resolution imagers (Reath et al. 2016).

Here we used ASTER Level 1T data (Precision Terrain Corrected Registered At-Sensor Radiance that contains calibrated at-sensor radiance, geometrically corrected and ortorectified into UTM projection. More specifically we analysed selected cloud-free TIR images (channel 13, centred at $\sim 11.3 \mu\text{m}$), with 90 m/pixel of spatial resolution, in order to locate the thermal anomalies associated to the activity detected by MODIS at the three volcanoes. Particular emphasis is given in discriminating between summit or lateral thermal anomalies and their association with the VRP measured by MODIS.

229

230 SO₂ flux (ϕSO_2) via Ozone Monitoring Instrument (OMI)

231 OMI is one of the four instruments on board of AURA NASA's satellite, dedicated to monitor
232 solar backscatter radiation over wavelengths spanning from 270 to 500 nm (visible and ultraviolet).
233 OMI is on orbit since the 1st October 2004 and provides daily global coverage through 14 orbits.
234 Each image has a complete swath of 2600 km and a nominal pixel spatial resolution of 13×24 km
235 at nadir. In this work we used the OMISO2 Product Level 2G that provide daily, global maps of
236 SO₂ vertical column density (in D.U.) at a resolution of $0.125^\circ \times 0.125^\circ$ (Krotkov et al. 2014).
237 This product is based on the Principal Component Analysis (PCA) algorithm (Li et al. 2017) and
238 provides four estimates SO₂ vertical column density, by assuming different centres of mass
239 altitudes (CMAs): at ~0.9 km (Planetary Boundary Layer, PBL), ~2.5 km (Lower tropospheric,
240 TRL), ~7.5 km (Middle tropospheric, TRM), and ~17 km (Lower stratospheric, STL), respectively
241 (see Carn et al. 2016).

242 When a volcanic plume is imaged by OMI, the amount (mass) of SO₂, hereby defined as MSO_2 ,
243 (in Tonnes), is quantified by using the equation proposed by Krueger et al. (1995),

$$244 \quad \text{MSO}_2 = 0.0285 \times \sum_{i=0}^n A_i \text{SO}_2_i \quad (2)$$

245 where A_i and SO_2_i represent the area (in km²) and the SO₂ vertical column density (in D.U.) of
246 each i^{th} OMI pixel sampling the volcanic plume (Fig. 3).

247 Conversion of SO₂ mass (MSO_2) into flux (ϕSO_2) is nontrivial, and requires detailed knowledge
248 of SO₂ removal rate into the atmosphere, as well as measurements of the wind field at the time of
249 each image acquisition (Theys et al. 2013). Due to the large amount of images and the different
250 conditions operating on the plumes of the three volcanoes, here we used a simplified approach

(Fioletov et al. 2015) whereby, under steady state emissions, the flux and the mass of SO₂ are related by:

$$\phi\text{SO}_2 \text{ (tonnes/day)} = \text{MSO}_2 / \tau \quad (3)$$

where (τ) is the lifetime of SO₂ into the atmosphere, assumed equal to 1 day (Beirle et al. 2014)

In order to quantify ϕSO_2 sourced by Stromboli, Batu Tara and Tinakula, we adopted a manual, contextual procedure that allows discarding anomalous pixels (artefacts) and/or volcanic plumes sourced by neighbour volcanoes. We first cropped a $10^\circ \times 10^\circ$ latitude-longitude box centred on each investigated volcano (Fig. 3). Hence, we calculated a local, contextual threshold, defined as $\mu + 3\sigma$, where μ and σ represent, the mean and the standard deviation of the pixels having SO₂ density lower than 1 D.U., respectively. All the pixels exceeding this threshold are thus flagged as SO₂-contaminated, and grouped into distinct clusters (groups of adjacent pixels). Finally, the visual inspection of all the images allow selecting only the specific clusters which are attributed, by the user, to the volcano of interest.

This last step was essential in many cases, where an SO₂ plume, located above or in proximity of the target volcano was in reality sourced by a neighbour volcano (Fig. 3). At Stromboli for example an automatic detection of SO₂ plumes would had been often triggered by the presence of large SO₂ emissions sourced by Mt. Etna drifting toward North (Fig. 3a, d). Similarly, in the Lesser Sunda region, the concurrent activity of several volcanoes located in proximity of Batu Tara (i.e. Lewotolo, Sirung and Egon mainly, located to south of Batu Tara; see Fig. 3b, e) sometimes produced SO₂-rich plumes extending over Batu Tara island (Fig. 3e). For these reasons, to obtain the most accurate time-series of ϕSO_2 and to avoid false detections, the visual inspection of all OMI images was found to be necessary, particularly for regions with multi-sources from active volcanoes.

According to the typical plume heights reported for the analysed volcanoes (typically less than 5 km), the calculation of MSO_2 has been retrieved by assuming the PBL and TRL layers only. Notably, it is well known that the values recorded at the two selected levels may diverge significantly (Flower et al. 2016). In general, the assumption of locating plume higher than the effective altitude could imply a substantial underestimate (up to 60%) and, locating the plume at lower altitude than that actually reached typically causes an overestimate greater than 100% (Hayer et al. 2016).

Results

In this section, we provide a description of VRP and ϕSO_2 time-series recorded at Stromboli, Batu Tara and Tinakula volcanoes by integrating our satellite data with previous research and/or reported visual observations and scientific communications regarding the investigated volcanoes (e.g. Global Volcanism Program - GVP reports; <http://www.volcano.si.edu>)

Time-series of satellite-derived VRP and ϕSO_2

The time-series of VRP and ϕSO_2 obtained for the three analysed volcanoes over the period 2000 and 2017 are shown in Fig. 4. Thermal data recorded for all three volcanoes display a quite similar range of values, with VRP spanning from less than 1 MW to about 1000 MW. However, there are differences in the persistence of the thermal anomalies, as well as in the frequency distribution of the data (Fig 4). Thermal detections at Stromboli are essentially continuous (Fig. 4a1) showing a bimodal distribution of VRP with modal values of ~5 MW and ~150 MW, respectively (Fig. 4c1). This contrasts with the signal recorded at Batu Tara that is characterised by a single, distinct phase of activity (Fig. 4b1) with a unimodal VRP distribution (mode equal to ~40 MW; Fig. 4b3). At

Tinakula, the thermal signals recorded suggest multiple phases of activity (Fig. 4c1) but with a unimodal VRP distribution peaking at 10 MW (Fig. 4c3).

The 2004–2017 time-series of ϕSO_2 also outline differences between each volcano, both in terms of magnitude and continuity of the emissions. Despite the continuous activity of Stromboli, few low-magnitude emissions are measured by OMI (modal value of ~ 100 tonnes/day, in the PBL; Fig. 4a2, a4), whereas higher magnitude and continuous emissions are recorded from Batu Tara (modal values of 130 to 450 tonnes/day in the TRL and PBL, respectively; cf. Fig. 4b2, b4). Sulphur dioxide emissions recorded at Tinakula essentially mimic the phases of thermal activity, with ϕSO_2 modal values of 30 and 100 tonnes/day in the TRL and PBL, respectively (cf. Fig. 4c2, c4). The recent event at Tinakula led to a peak of ϕSO_2 ($>10,000$ tonnes/day) recorded in October 2017.

Stromboli's radiative flux shows a quite continuous and stable trend with values less than 20–30 MW, interrupted by periods with VRP generally greater than 100 MW and peaking at 4600 MW (Fig. 4a1). Previous work shows that the lower thermal emissions are related to the “normal” mild explosive activity, whereas the high VRP periods coincide with the three effusive flank eruptions (e.g., Calvari et al. 2014; Coppola et al. 2014; Valade et al. 2016; Ripepe et al. 2017). Further episodic measurements greater than 50–100 MW are linked to summit overflows and/or short fountaining episodes that occurred during 2009–2014 (black arrows in Fig. 4a1; cf. Calvari et al. 2014; Valade et al. 2016). Notably, our ϕSO_2 data, suggest that the continuous degassing associated to the normal activity of Stromboli (~ 150 tonnes/day; Burton et al. 2009) was not clearly identifiable in the OMI images. On the other hand, during the periods characterised by the occurrence of summit overflows (e.g. Dec 2010 – Apr 2013; Calvari et al. 2014; Fig 4a2) as well

as during the two effusive flank eruptions (e.g. Feb 2007, Aug-Oct 2014), the volcanic plume was clearly sourced by Stromboli reaching peak ϕSO_2 of 480 tonnes/day (at PBL level).

Data from Batu Tara shows the first signs of low thermal activity (1–2 MW) between July and December 2006, followed by continuous activity between 2007 and 2016. From early January 2007 the thermal activity increased progressively to reach a peak of 490 MW on February 2007 (Fig. 4b1). According to 2007–2008 reports, a channelised lava flow was emplaced along the scar, reaching the sea and building a lava delta (GVP 2007). This effusive activity was accompanied by explosive activity characterised by the emission of ash-rich volcanic plumes that recurrently reached an altitude of about 3–4 km (GVP 2007). Following this, the thermal record displays a slow but gradual reduction of activity (from 100–200 MW on 2007 to about 20–30 MW on 2013). This reduction was confirmed by field observations in 2014, which reported the absence of lava effusion and that explosive activity was confined to the summit crater (Gaudin et al. 2017). On 23 October 2016, the thermal activity drastically decreased to less than 1 MW suggesting the end of the eruption (Fig. 4b1).

Reports from the Darwin Volcanic Ash Advisory Centre (VAAC) throughout the whole eruption indicate the presence of a volcanic plume over Batu Tara at an altitude of 2–4 km (GVP 2008). Accordingly, in the following sections, the TRL layer is considered the most appropriate for retrieving ϕSO_2 from Batu Tara (see Fig. 4b2, b4).

The first detection of SO_2 -rich plume over Batu Tara was on 26 July 2005 (<100 tonnes/day), about one year prior to the beginning of thermal activity in July 2006 (see blue and red lines in Fig. 4b1, b2). The ϕSO_2 time-series essentially mimics the thermal trend, with both describing a short waxing phase, followed by a slow waning phase until the end of 2016 (Fig. 4b1, b2). It is

interesting to note that during 2016 and during the first part of 2017, small plumes were still detected over Batu Tara, despite no evidence of surface activity in the thermal data (Fig. 4b1). The last ϕSO_2 detection was recorded on 7 April 2017 (Fig. 4b2).

At Tinakula, the heat flux time-series defines at least three main phases of activity, interrupted by year-long periods lacking thermal alerts (Fig. 4c1). During the 2000–2001 a first phase of low thermal emission can be identified as characterised by sporadic and low-magnitude thermal detections (< 20 MW). Conversely, the relatively long-lasting phases occurring in 2006–2012 (eventually subdivided into distinct stages) show thermal emissions often exceeding 100 MW (with a largest value of 1120 MW, 11 Feb 2006; Fig. 4c1). The 2010–2012 period was defined by an increasing trend, with a maximum VRP (~ 200 MW) that reached on July 2012. This recorded thermal behaviour could be reconciled with a strombolian-type activity, encompassing from persistent degassing to high-explosive phases, as testified by available reports (GVP 2003, 2006). Between 2013 and 2017, our measurements suggest the total absence of VRP and ϕSO_2 detections (Fig. 4c). However, after about five years of repose, a new small (2 MW) thermal anomaly was detected on 19 October 2017 (Fig. 4c1). The renewed thermal activity was immediately followed by the VEI 3 explosive phase on 21 October (GVP 2017). The thermal emissions from this short explosive phase were detected for a few days only, and reached a maximum VRP of 20 MW.

The ϕSO_2 time-series of Tinakula between 2005 and 2017 overlap with the timing of the eruptive phases depicted by the VRP data. The first clear OMI data coincides to the thermal onset on 11 February 2006 and is followed on 12–13 February by peak values of up to 2750 tonnes/day, using the TRL level. This level appears appropriate because scientific communications report the

occurrence of VEI 2 explosive eruptions reaching an altitude of less than 5 km (GVP 2013, Eruptive History; <https://volcano.si.edu/volcano.cfm?vn=256010>).

Between 2007 and 2012, there were no ash-advisory reports regarding Tinakula, suggesting a low-altitude emission or, otherwise, an ash-free volcanic plume. According to the PBL estimates, the MSO₂ measured in this period ranged from 50 to about 450 tonnes/day, showing a slight increase during 2010 and 2011. However, gas emissions declined throughout 2012, with the last OMI detection coinciding with the last thermal alert, on 21 November 2012 (Fig. 4c2). On 21–23 October 2017, the reawakening of Tinakula produced a peak ϕ SO₂ of ~42,000 tonnes/day, related to a 11 km-height volcanic column from the VEI 3 explosion (NDMO Report 2017; GVP 2017).

VRP distribution and activity regimes

Stromboli volcano is characterised by a clear bimodal distribution of VRP values, with two groups of data separated at approximately 50 MW (Fig. 5a). As reported in previous works (see Coppola et al. 2012, 2014), the two groups can be related to the summit explosive- and flank effusive- activity, respectively (Fig. 5a). Actually, the ASTER images (Fig. 5a1–4) illustrate that the low radiating group (values less than about 50 MW) is associated to intra-crater thermal anomalies, likely related to mild-explosive activity at the summit vents. On the other hand, during sporadic detection of VRP >100 MW associated to summit overflows (cf. Online Resource 2; 2010–2012), the thermal anomaly extended from the crater area towards the coast (Fig. 5a3).

During the effusive eruptions, the heat flux typically exceeds 100 MW, and the ASTER images reveals a flank thermal anomaly, extending along the entire length of the Sciara del Fuoco, whose origin (vent) is slightly shifted towards the NE from the crater terrace, which in turn appear cold (Fig. 5a4). The shift of this thermal anomaly clearly enhance how the effusion of lava from a lateral

vent was able to drain the upper portion of the magmatic system feeding the typical strombolian activity at the summit crater.

Conversely, Batu Tara and Tinakula histograms (Fig. 5b, c) are characterised by a rough unimodal distribution showing VRP modal peaks at 40 MW and 10 MW, respectively.

At Batu Tara, VRP spans from 1 MW to about 500 MW, with a arithmetic mean of 30 MW, close to the modal peak shown in Fig. 5b. Notably, VRP values greater than 10 MW are associated to summit activity producing minor lava flows channelled into the scarp area, and causing an extension of the observed TIR anomaly (Fig. 5b2, b3). The ASTER image of 9 December 2015, acquired during a low radiant flux phase (cf. Online Resource 2), suggests that values below 10 MW are associated with weak thermal activity confined exclusively inside the summit vent (Fig. 5b4).

The analysis of ASTER images acquired over Tinakula suggests that the VRP derived from MIROVA is associated to an intra-crater thermal anomaly, sometime extending down the scarp area (Fig 5c2, c3). This kind of thermal anomalies are likely associated to mild explosive activity at the summit crater eventually evolving to overflows as suggested by the ASTER image acquired on 11 September 2011 (Fig. 5c3). Given the lack of evidences for the occurrence of flank eruptions at Tinakula, we are confident that the onset of the eruption on 11 February 2006 (with peak VRP of ~1120 MW) was related to powerful effusive eruption from summit crater, producing a lava flow that reached the lower portions of the *Sciara del Fuoco*-like scarp.

From the analysis of VRP and ASTER images, we may infer that the bimodal distribution of VRP recorded at Stromboli reflects two distinct eruptive regimes associated to (i) the typical mild-

explosive summit activity and (ii) the flank effusive episodes, respectively. This bimodal behaviour is not observed at Batu Tara and Tinakula volcanoes, which have not experienced lateral effusion over the investigated period. Hence, the unimodal distribution of the radiative power dataset seems to reflect summit activity spanning from effusive outflows to explosive ash-rich activity (cf. GVP 2007, 2012).

Discussion

The VRP and ϕSO_2 time-series presented above offer an unique opportunity to compare the eruptive behaviours of the three volcanoes on a decade-long timescale. In order to homogenise the two datasets we calculated the arithmetic means of VRP and ϕSO_2 , over monthly intervals (Fig. 6). Hence, we integrated over time the two monthly fluxes to obtain the cumulative Volcanic Radiant Energy (cumVRE, in Joules) and the cumulative SO_2 mass (cum SO_2 , in tonnes) throughout the whole analysed period (Fig. 7). We recognise that this procedure may be inaccurate in case of extreme isolated events, such as the VEI 3 explosion of Tinakula on 21 October 2017. However, for long-term analysis this methodology minimizes the effects related to poor acquisition conditions (i.e. cloud coverage and geometry conditions among others; cf. Online Resource 1) and allows the eruptive trends to be preserved and compared.

We now focus on two main aspects that reveal the different eruptive behaviour of the three volcanoes: (i) the long-term eruptive trends and cumulative emissions and (ii) the ϕSO_2 / VRP ratio.

Long-term eruptive trends and cumulative emissions

As described previously, Stromboli's thermal activity is characterised by a bimodal distribution (Fig. 5a), representing the “normal” strombolian activity ($VRP < 50$ MW) and the effusive activity (summit overflows or flank eruptions with $VRP > 50$ MW), respectively. These two thermal regimes are also discernible in the monthly time-series (Fig. 6a1) where the persistent low level thermal emission, attributed to the strombolian activity, is interrupted by peaks during effusive episodes (cf. Coppola et al. 2012). On the other hand, ϕSO_2 time-series (Fig. 6a2) reveals that the “normal” strombolian activity (~ 150 tonnes/day; Burton et al. 2009) is essentially undetected by our analysis of the OMSO₂ Level 2G images, likely because emissions are below the detection limit of the sensor. The visual inspection of all OMI images and the manual selection of volcanic plume sourced by Stromboli, may explain the discrepancy between our results and those obtained by Carn et al. (2017), who measured, a long-term (2005-2015) average SO₂ emission of ~ 180 tonnes/day. Possibly, the automatic detection method used by Carn and co-authors (2017), based on pixel averaging or oversampling procedure, included data contaminated by the Etna's plume which were wrongly attributed to Stromboli. Our analysis detected an SO₂ plumes exclusively during the two major flank eruptions of Stromboli, as well as during a few periods characterised by more sustained activity and summit overflows (cf. Fig. 4a2).

The cumulative data indicate that during the whole analysed period (13 years), Stromboli radiated $\sim 4.1 \times 10^{15}$ J of heat, and emitted a total OMI-derived SO₂ mass of only 12.5×10^3 tonnes (Fig. 7a). However, over the same time window, the undetected normal activity (corresponding to about 95% of the days over the 13 year period) should have emitted approximately 712×10^3 tonnes of SO₂ into the atmosphere (assuming a steady flux of ~ 150 tonnes/day rate; Burton et al. 2009). This strong imbalance illustrates the substantial contribution of the mild-strombolian explosions and the passive degassing to the total degassing budget of Stromboli. Paradoxically, the cumulative

trends (Fig. 7a) show a very good correspondence, indicating that the long-term thermal emission of Stromboli is dominated by the “out of the ordinary” activity, or rather by flank eruptions and summit overflows (for which we have the only SO₂ detections in the OMI data).

The trend depicted from monthly VRP records of Batu Tara shows a rapid waxing phase followed by a slow waning phase characterised by an exponential decay (Fig. 6b1). The monthly ϕ SO₂ trend displays a similar pattern, although the waxing phase starts some months earlier, and the waning trend ends some months later (Fig. 6b2). Nevertheless, the cumulative curves (Fig. 7b) show a good correlation ($R^2 = 0.9766$), suggesting that activity at Batu Tara was driven by a progressive decrease in the overpressure from a closed magma chamber (e.g. Machado 1974; Scandone 1979; Wadge 1981; Stasiuk et al. 1993). Typically, such exponentially-decreasing trends are observed during basaltic effusive eruptions (e.g. Wadge 1981, Rowland et al., 2003, Harris et al., 2000), although there are exponential trends have been recorded also during the effusion of silicic lava flows and domes (e.g. Mastin et al. 2008; Pallister et al., 2010; Coppola et al. 2017b). The decay time constant of this type of trend is controlled by the viscosity and bulk modulus of the magma, as well as by the size and geometry of the plumbing system (e.g. Wadge 1981, Rowland et al., 2003; Mastin et al. 2008), with large, deep magma chambers typically producing long-lasting decay (Machado 1974, Scandone 1979). The longevity of the exponential trend recorded at Batu Tara (~9 years) is extraordinary, and there are no similar records of long declining trend from the MODIS era (2000–2018). To our knowledge, only the 1943–1952 Paricutin eruption was characterised by a similar decay constant over a total duration of nine years (Scandone 1979). Notably, the previous eruption of Batu Tara (1847–1852) lasted six years, a duration quite similar to the 2007–2016 eruption. As pointed out by Scandone (1979), the exponential trend also indicates that after the eruption started, the magma reservoir was not fed by new magma (or that

resupply was insignificant in comparison to the output rate). Our data also reveal that the ϕSO_2 were initially detected several months before the thermal onset of the eruption (Fig. 6b1, 6b2), thus suggesting that precursory degassing activity may have preceded the arrival of magma at the surface. Such a precursor would be consistent with a gas-magma decoupling during the formation of the vertical magma conduit.

The eruption of Tinakula started suddenly on 11 February 2006, reaching a VRP of 1120 MW and a ϕSO_2 of 1562 tonnes (Fig. 4). Following this highly-energetic beginning, both VRP and ϕSO_2 decreased rapidly, to remain at lower levels throughout 2007 and 2008. After a pause of more than one year, the thermal activity resumed in 2010, showing an escalation of VRP that culminated in April–July 2012 (Fig. 6c1, c2). This thermal trend suggests a slow but progressive increase of magma discharge rate during eruption, thereafter followed by a rapidly waning phase ending in November 2012. According to Scandone (1996), the gradual intensification of the eruptive activity is typical of explosive eruptions, although this trend has now also been recognised during basaltic effusive eruptions (e.g. Reath et al. 2016; Harris et al. 2011, Coppola et al. 2017c). Scandone (1996) explains the relatively slow waxing trend and rapid waning phase by a delayed bubble growth within the magma chamber, which mainly depends on magma composition and depth of the reservoir.

Notably, the rise in the 2011–2012 Tinakula thermal activity was not accompanied by an equivalent increase of ϕSO_2 (Fig. 6c2), suggesting a gradual modification of the gas/magma balance throughout this stage. The cumulative trends highlight this feature, clearly showing a sharp decoupling of CumVRE and CumSO₂ after 2011 (Fig. 7c). During 2007–2010, the two cumulative curves follow each other closely (suggesting a syn-eruptive degassing) but, after 2011 there is a

clear mismatch between the two signals, with the rapid growth of CumVRE not being accompanied by CumSO₂ (Fig. 7c).

From November 2012 to October 2017, the absence of VRP and ϕ SO₂ detections suggests a complete cessation of activity (cf. Fig. 4c1, 2 with Fig. 7c). This five-year long period of rest was dramatically interrupted in October 2017 when the VEI 3 eruption produced $\sim 40 \times 10^3$ tonnes/day of sulphur dioxide, the highest ϕ SO₂ value of the whole Tinakula dataset (Fig. 4c2).

ϕ SO₂ / VRP ratio: a proxy for degassed/erupted magma budget

Further interpretation of the eruptive behaviours can be considered by linking ϕ SO₂ and VRP to the source process characteristics of (i) the rate at which the magma is supplied to the level for SO₂ exsolution (Q_{in}), and (ii) the rate at which the magma reaches the surface and is erupted (Q_{out}), to release detected thermal radiation. Previous research has demonstrated how this approach enables to investigate the mass partitioning during eruptive phases (endogenous versus exogenous growth) and the magma plumbing systems feeding the activity at the surface (Francis et al. 1993; Harris and Stevenson, 1997; Steffke et al. 2011; Coppola et al. 2016d). In this framework, the theoretical flux ϕ SO₂ (in tonnes/day) can be calculated by a simplified version of the petrological method (Shinohara 2008),

$$\Phi SO_2 = (Q_{in} \cdot 2X_S) \cdot \frac{86400}{1000} \quad (4)$$

where Q_{in} is the magma supply rate (kg/s) and X_S is the weight fraction of sulphur (S) within the undegassed melt.

On the other hand, VRP can be related to Q_{out} through an appropriate conversion coefficient that considers how the lava flux is accommodated by the surface extent and temperature of the active lavas (Harris and Baloga 2009). For any rheological case, a single parameter called radiant density

(c_{rad}), can be used to describe the spreading and cooling properties of an active lava (Coppola et al. 2013), so that

$$VRP = \frac{Q_{out}}{\rho_m} \cdot c_{rad} \quad (5)$$

where Q_{out} is the magma output rate (kg/s), ρ_m is the magma density (kg/m³), and c_{rad} (J/m³) is an empirical best-fit parameter that relates the lava discharge rate to the thermal radiation.

Under the condition that all the magma supplied at shallow levels is able to degas and then erupts (i.e., $Q_{in} = Q_{out}$), the equations 1 and 2 can be combined to give, for any volcanic system, a linear relationship between ϕSO_2 and VRP, representing “balanced emissions”,

$$\Phi SO_2 = \left(\frac{86400 \cdot \rho \cdot 2X_S}{1000 \cdot c_{rad}} \right) \cdot VRP = k_{bal} \cdot VRP \quad (6)$$

where the coefficient k_{bal} defines the slope of the ϕSO_2 versus VRP relationship (in tonnes day⁻¹/MW, for simplicity). The exact value of k_{bal} depends on the chemical and physical properties of the erupted magma and may vary from case to case. Considering this variability, here we use a wide range of parameters that encompass the typical density ($\rho = 2500$ kg/m³; Bottinga and Weill 1972), sulphur content ($S = 500$ – 2500 ppm; Shinohara 2008) and radiant density ($c_{rad} = 0.5$ – 2×10^8 J/m³; Coppola et al. 2013) of basaltic to basaltic-andesitic magmas (as at Stromboli, Batu Tara and Tinakula).

On a ϕSO_2 versus VRP plot, the resulting range of k_{bal} (of 1.1 to 21.6 tonnes day⁻¹/MW) defines a region that corresponds to the 1:1 ratio between Q_{in} and Q_{out} (yellow field in Fig. 8a). Accordingly, any measurement of the ϕSO_2 /VRP ratio above this value, is likely to indicate “excess” SO₂ degassing, that is more magma is degassed than is erupted. The opposite is true (low ϕSO_2 /VRE ratio) when more magma is erupted than degassing, giving origin to a “deficit” of SO₂ degassing. The standard explanation for the former case is that some of the magma is intruded and

not erupted (e.g. Dzurisin 2001), and for the latter that magma that has been previously degassed is involved (e.g., Steffke et al., 2011). We here term the former eruption of 'gas-rich' magma, and the latter 'gas-poor'.

The monthly emissions derived from OMI and MODIS data are plotted in Fig. 8b, where the datasets of Stromboli, Batu Tara and Tinakula define overlapping but distinct fields. For each volcano, the temporal evolution of measured emission $\phi\text{SO}_2/\text{VRP}$ ratio is also showed in Fig. 6#3.

From this analysis, we may outline:

Stromboli's dataset can be divided into two sub-groups: (1) a thermally energetic group ($\text{VRP} > 10 \text{ MW}$) falling essentially within the field of gas-poor eruptions, and (2) a moderately energetic group, falling within the field of balanced emissions (Fig. 8b). As previously described, OMI was unable to detect the SO_2 plumes sourced by the normal strombolian activity. Therefore, the observed $\phi\text{SO}_2/\text{VRP}$ ratio for Stromboli, refers exclusively to the phases of lava emission characterising the two major flank eruptions (highly energetic) and the episodic summit overflows (moderately energetic). The two flank eruptions produce the lowest $\phi\text{SO}_2/\text{VRP}$ ratio of the time-series (Fig. 6a3), a clear indication of the eruption of degassed (gas-poor) lava. This is consistent with the reported deficit of SO_2 degassing recorded during the 2007 eruption (Burton et al. 2009). The gravity-driven magmastatic model proposed by Ripepe et al. (2015) provides an explanation for this imbalance, whereby the flank eruptions of Stromboli essentially drain the superficial, degassed magma reservoir, confined between the crater terrace and the effusive vent (e.g. Burton et al. 2009; Calvari et al. 2011; Valade et al. 2016; Ripepe et al. 2017, Zakšek et al. 2015). Summit overflows are characterised by moderately gas-poor to balanced $\phi\text{SO}_2/\text{VRP}$ ratio (Fig. 8b), which is consistent with the fact that they represent a transient regime, separating the strombolian (gas-rich) and the flank (gas-poor) activity (see Coppola et al. 2012).

Batu Tara's dataset plot mostly within the balanced field (Fig. 8b) with only a few low-thermal-energy data toward the gas-rich field. The time-series (Fig. 6b3) reveals that these low-energy, gas-rich measurements correspond to the precursory phase (2005–2006), characterised by the first arrival of magmatic volatiles at the surface. During and after the onset of the eruption, the $\phi\text{SO}_2/\text{VRP}$ ratio does not show any significant long-term pattern (Fig. 6b3), indicating the absence of gas accumulation/separation and an overall syn-eruptive degassing (Parfitt and Wilson, 1995). This behaviour, together with the coherent exponential trends (Fig. 7b), suggests that the Batu Tara eruption tapped a pressurised magma chamber (Wadge 1981) located below the SO_2 exsolution level, and that magma ascent was sufficiently fast to limit the separation of the gas phase along the central conduit (Parfitt and Wilson 1995).

Tinakula's dataset exhibit the largest variability of the $\phi\text{SO}_2/\text{VRP}$ ratio and contains the highest value (of $\sim 10,000$ Tonnes day⁻¹/MW recorded during the VEI 3 eruption, October 2017) as well as some data falling in the moderately gas-poor region (Fig. 8b). The extreme ratio of October 2017 (Fig. 6c3) suggests that this event was possibly preceded by a period of gas accumulation at depth. Interestingly, between 2006–2012, the gas/thermal ratio gradually declined, evolving from moderately gas-rich (2006–2007) to gas-poor conditions (2011–2012; Fig. 6c3). This terminal gas-depleted stage corresponds to the progressive intensification of thermal emission (Fig. 6c3), likely resulting from an increase in magma discharge rate. According to Scandone (1996), this style of evolution may be promoted by a volatile-saturated magma confined within a rigid magma chamber. In this way, the escalation of observed discharge rate can be driven by an increase in the rate of vesiculation by the progressive emptying of the reservoir enhancing magma decompression during the eruptions. Consequently, high discharge rates favour the tapping of increasingly deeper levels in a zoned reservoir with possible eruption of magma with a lower gas content (Spera, 1984;

Blake and Ivey 1986). This seems to be exactly the case for Tinakula, where the slow eruption of a gas-rich magma stored at the top of the reservoir (2006–2007 phase), possibly unloaded the residual degassed magma, stored at lower levels and erupted during the last stage of activity (2011–2012 phase).

Conclusions

Batu Tara and Tinakula are two poorly known volcanoes displaying morphologies and short-term activity very similar to Stromboli. However, our analysis of satellite data reveals that over timescales of several years, the three volcanoes display quite different eruptive behaviours in terms of (i) persistence and magnitude of thermal and degassing fluxes (VRP and ϕSO_2 , respectively), (ii) long-term eruptive trends and (iii) ϕSO_2 /VRP ratios. These contrasting behaviours are likely attributable to differences in the associated magmatic systems. The efficient, well-developed plumbing system of Stromboli allows the magma column to reach very shallow depths (just below the crater terrace) and persistently degas. These results in the continuous detection of low thermal anomalies, and the continuous emission of gas, albeit at levels undetectable by the OMI sensor. However, flank eruptions are able to drain the top of the magmatic column, with the consequent effusion of degassed magma. Conversely, the eruptive trends recorded at Batu Tara are indicative of a less-well developed magmatic system, lacking a persistently-fed shallow conduit, and suggesting the involvement of a deep magma chamber (below the SO_2 exsolution level), possibly erupting every hundred years. Finally, the behaviour of Tinakula may be explained by intermittent eruptions (every few years) from a volatile-zoned magma chamber, possibly located at intermediate depths (i.e. around the SO_2 exsolution level). Notably, the last five years of activity

at Tinakula indicates a closed system behaviour, with a possible gas accumulation that was erupted during the VEI 3 explosive event of October 2017.

Our results outline the potential of comparative analysis of long-term eruptive trends. The satellite data with their continuous, long-lasting, global coverage represent an invaluable resource that can inform on eruption processes at unmonitored volcanoes. The combined analysis of VRP and ϕSO_2 constitutes a promising and powerful tool to decrypt major changes in the eruptive behaviour of any active volcano, thus adding a fundamental contribution for the evaluation of evolving volcanic hazards.

Acknowledgments

MIROVA is a collaborative project between the Universities of Turin and Florence (Italy), and is supported by the Italian Civil Protection Department. We acknowledge the LANCE-MODIS system (<http://lance-modis.eosdis.nasa.gov/>) for providing Level 1BMODIS data. ASTER images are visible on the Geological Survey of Japan portal (<https://www.gsj.jp/>); the data are courtesy of USGS and available at <http://earthexplorer.usgs.gov/>. Analyses and visualizations used in Figure S1 were produced with the Giovanni online data system, developed and maintained by the NASA GES DISC (<http://disc.sci.gsfc.nasa.gov/>). The constructive comments of three unknown reviewers have been truly appreciated. We warmly thank the Associate Editor M. R. James that with its inspired suggestions contributed to greatly improve the quality of the manuscript and motivated us to publish this research.

References

Aiuppa A, Bertagnini A., Métrich N, Moretti R, Di Muro A, Liuzzo M, Tamburello GA (2010) A model of degassing for Stromboli volcano. *Earth Planet Sci Lett* 295: 195–204. doi:10.1016/j.epsl.2010.03.040

644 Aiuppa A, de Moor JM, Arellano S, Coppola D, Francofonte V, Galle B, Giudice G, Liuzzo M,
 645 Mendoza E, Saballos A, Tamburello G, Battaglia A, Bitetto M, Gurrieri S, Laiolo M, Mastrolia A,
 646 Moretti M (2018) Tracking formation of a lava lake from ground and space: Masaya volcano
 647 (Nicaragua), 2014–2017. *Geochem Geophys Geosyst* 19 (2): 496-515.
 648 <https://doi.org/10.1002/2017GC007227>
 649
 650 Allard P, Carbonnelle J, Métrich N, Loyer H, Zettwoog P (1994) Sulphur output and magma
 651 degassing budget of Stromboli volcano. *Nature* 368: 326-330. doi:10.1038/368326a0
 652
 653 Allard P, Aiuppa A, Burton M, Caltabiano T, Federico C, Salerno G, La Spina A (2008) Crater
 654 gas emissions and the magma feeding system of Stromboli volcano. In: Calvari S, Inguaggiato S,
 655 Puglisi G, Ripepe M, Rosi M (ed), *Learning from Stromboli*, AGU Geophysics Monograph Series,
 656 182, Washington DC, pp. 65–80. doi: 10.1029/182GM07
 657
 658 Andres RJ, Kasgnoc AD (1998) A time-averaged inventory of subaerial volcanic sulfur emissions.
 659 *J Geophys Res* 103 (D19): 25251-25261.
 660
 661 Barberi F, Rosi M, Sodi A (1993) Volcanic hazard assessment at Stromboli based on review of
 662 historical data. *Acta Vulcanol* 3:173-187.
 663
 664 Barrière J, Oth A, Theys N, d'Oreye N, Kervyn F (2017) Long-term monitoring of long-period
 665 seismicity and space-based SO₂ observations at African lava lake volcanoes Nyiragongo and

666 Nyamulagira (DR Congo). *Geophys Res Lett* 44(12): 6020-6029.
667 <http://dx.doi.org/doi:10.14470/XI058335>
668

669 Beirle S, Hormann C, Penning de Vries M, Dorner S, Kern C, Wagner T (2014) Estimating the
670 volcanic emission rate and atmospheric lifetime of SO₂ from space: a case study for Kīlauea
671 volcano, Hawai‘i. *Atmos Chem Phys* 14: 8309-8322. <https://doi.org/10.5194/acp-14-8309-2014>
672

673 Biggs J, Ebmeier SK, Aspinall WP, Lu Z, Pritchard ME, Sparks RSJ, Mather TA (2014) Global
674 link between deformation and volcanic eruption quantified by satellite imagery. *Nat Commun* 5:
675 3471. doi: [10.1038/ncomms4471](https://doi.org/10.1038/ncomms4471)
676

677 Biggs J, Pritchard ME (2017) Global volcano monitoring: What does it mean when volcanoes
678 deform? *Elements* 13(1): 17-22. <https://doi.org/10.2113/gselements.13.1.17>
679

680 Blake S, Ivey GN (1986) Density and viscosity gradients in zoned magma chambers, and their
681 influence on withdrawal dynamics. *J Volcanol Geotherm Res* 30: 201-230.
682 [https://doi.org/10.1016/0377-0273\(86\)90055-7](https://doi.org/10.1016/0377-0273(86)90055-7)
683

684 Bottinga Y, Weill DF (1972) The viscosity of magmatic silicate liquids; a model calculation. *Am*
685 *J Sci*: 272 (5): 438-475. [https://doi.org/10.1016/0377-0273\(86\)90055-7](https://doi.org/10.1016/0377-0273(86)90055-7)
686

687 Burton MR, Caltabiano T, Murè F, Salerno GG, Randazzo D (2009) SO₂ flux from Stromboli
 688 during the 2007 eruption: results from the FLAME network and traverse measurements. J Volcanol
 689 Geotherm Res 182 (3–4): 214–220. <https://doi.org/10.1016/j.jvolgeores.2008.11.025>
 690
 691 Calvari S, Spampinato L, Bonaccorso A, Oppenheimer C, Rivalta E, Boschi E (2011). Lava
 692 effusion — A slow fuse for paroxysms at Stromboli volcano? Earth Planet Sci Lett 301 (1–2): 317-
 693 323. <https://doi.org/10.1016/j.epsl.2010.11.015>
 694
 695 Calvari S, Bonaccorso A, Madonia P, Neri M, Liuzzo M, Salerno GG, Behncke B, Caltabiano T,
 696 Cristaldi A, Giuffrida G, La Spina A, Marotta E, Ricci T, Spampinato L (2014) Major eruptive
 697 style changes induced by structural modifications of a shallow conduit system: the 2007–2012
 698 Stromboli case. Bull Volcanol 76: 841. <https://doi.org/10.1007/s00445-014-0841-7>
 699
 700 Carn SA, Clarisse L, Prata AJ (2016) Multi-decadal satellite measurements of global volcanic
 701 degassing. J Volcanol Geotherm Res 311: 99–134.
 702 <https://doi.org/10.1016/j.jvolgeores.2016.01.002>
 703
 704 Carn SA, Fioletov VE, McLinden CA, Li C, Krotkov NA (2017) A decade of global volcanic SO₂
 705 emissions measured from space. Sci Rep 7: 44095. doi:10.1038/srep44095
 706
 707 Chaussard E, Amelung F, Aoki Y (2013) Characterization of open and closed volcanic systems in
 708 Indonesia and Mexico using InSAR time series. J Geophys Res SE 118: 3957–3969.
 709 <https://doi.org/10.1002/jgrb.50288>

710

711 Cook HJ, Koraua BL, McConachy TF (2012) Observations of Tinakula Volcano, 10 May 2012,
712 Solomon Islands (-10.38°S / 165.8°E), Informal report, 12 pp.

713

714 Coppola D, Cigolini C (2013) Thermal regimes and effusive trends at Nyamuragira volcano (DRC)
715 from MODIS infrared data. Bull Volcanol 75 (8): 1-15. [https://doi.org/10.1007/s00445-013-0744-](https://doi.org/10.1007/s00445-013-0744-z)
716 [z](https://doi.org/10.1007/s00445-013-0744-z)

717

718 Coppola D, Piscopo D, Laiolo M, Cigolini C, Delle Donne D, Ripepe M (2012) Radiative heat
719 power at Stromboli volcano during 2000–2011: Twelve years of MODIS observations. J Volcanol
720 Geotherm Res 215-216: 48-60. <https://doi.org/10.1016/j.jvolgeores.2011.12.001>

721

722 Coppola D, Laiolo M, Piscopo D, Cigolini C (2013) Rheological control on the radiant density of
723 active lava flows and domes. J Volcanol Geotherm Res 249: 39–48.
724 <https://doi.org/10.1016/j.jvolgeores.2012.09.005>

725

726 Coppola D, Laiolo M, Delle Donne D, Ripepe M, Cigolini C (2014) Hot-spot detection and
727 characterization of strombolian activity from MODIS infrared data. Int J Remote Sens 35 (9):
728 3403-3426. <https://doi.org/10.1080/01431161.2014.903354>

729

730 Coppola D, Macedo O, Ramos D, Finizola A, Delle Donne D, del Carpio J, White R, McCausland
731 W, Centeno R, Rivera M, Apaza F, Ccallata B, Chilo W, Cigolini C, Laiolo M, Lazarte I, Machaca
732 R, Masias P, Ortega M, Puma N, Taipe E (2015) Magma extrusion during the Ubinas 2013-2014

eruptive crisis based on satellite thermal imaging (MIROVA) and ground-based monitoring. J
Volcanol Geotherm Res 302: 199–210. <https://doi.org/10.1016/j.jvolgeores.2015.07.005>

Coppola D, Laiolo M, Cigolini C (2016a) Fifteen years of thermal activity at Vanuatu’s volcanoes
(2000–2015) revealed by MIROVA. J Volcanol Geotherm Res 322: 6–19.
<https://doi.org/10.1016/j.jvolgeores.2015.11.005>

Coppola D, Laiolo M, Lara L, Cigolini C, Orozco G (2016b) The 2008 “silent” eruption of
Nevados de Chillán (Chile) detected from space: Effusive rates and trends from the MIROVA
system. J Volcanol Geotherm Res 327: 322–329. doi:10.1016/j.jvolgeores.2016.08.016

Coppola D, Laiolo M, Cigolini C, Delle Donne D, Ripepe M (2016c) Enhanced volcanic hot-spot
detection using MODIS IR data: results from the MIROVA system. In: Harris AJL, De Groeve T,
Garel F, Carn SA (ed), Detecting, Modelling, and Responding to Effusive Eruptions, Geological
Society, London, Special Publication 426. <https://doi.org/10.1144/SP426.5>

Coppola D, Champion R, Laiolo M, Cuoco E, Balagizi C, Ripepe M, Cigolini C, Tedesco D (2016d)
Birth of a lava lake: Nyamulagira volcano 2011–2015. Bull Volcanol 78. doi:10.1007/s00445-016-
1014-7

Coppola D, Ripepe M, Laiolo M, Cigolini C (2017a) Modelling satellite-derived magma discharge
to explain caldera collapse. Geology 45 (6): 523–526: <https://doi.org/10.1130/G38866.1>

756 Coppola D, Laiolo M, Franchi A, Massimetti F, Cigolini C, Lara LE (2017b) Measuring effusion
 757 rates of obsidian lava flows by means of satellite thermal data. *J Volcanol Geotherm Res* 347, 82-
 758 90. <https://doi.org/10.1016/j.jvolgeores.2017.09.003>
 759
 760 Coppola D, Di Muro A, Peltier A, Villeneuve N, Ferrazzini V, Favalli M, Bachèlery P, Gurioli L,
 761 Harris AJL, Moune S, Vlastélic I, Galle B, Arellano S, Aiuppa A (2017c) Shallow system
 762 rejuvenation and magma discharge trends at Piton de la Fournaise volcano (La Réunion Island).
 763 *Earth Planet Sci Lett* 463: 13-24. <https://doi.org/10.1016/j.epsl.2017.01.024>
 764
 765 Davies HL, Keene JB, Hashimoto K, Joshima M, Stuart JE, Tiffin DL (1986) Bathymetry and
 766 Canyons of the western Solomon Sea. *Geo-Marine Lett* 6 (4): 181-191.
 767 <https://doi.org/10.1007/BF02239579>
 768
 769 Davies HL, Bani P, Black P, Smith I, Garaebiti E (2005) Geology of Oceania (including Fiji, Ping
 770 and Solomons). In: Selley RC, Cocks LRM, Plimer IR (ed), *Encyclopedia of Geology*, Oxford
 771 Elsevier, 4, pp. 109-123.
 772
 773 De Astis G, Ventura G, Vilardo G (2003) Geodynamic significance of the Aeolian volcanism
 774 (Southern Tyrrhenian Sea, Italy) in light of structural, seismological, and geochemical data.
 775 *Tectonics* 22(4):1040. <https://doi.org/10.1029/2003TC001506>
 776
 777 Dean KG, Servilla M, Roach A, Foster B, Engle K (1998) Satellite monitoring of remote volcanoes
 778 improves study efforts in Alaska. *EOS, Transactions of the American Geophysical Union* 79: 422–
 779 423. <https://doi.org/10.1029/98EO00316>

Dzurisin D (2001) A comprehensive approach to monitoring volcano deformation as a window on the eruption cycle. *Rev Geophys* 41 (1). <https://doi.org/10.1029/2001RG000107>

Ebmeier SK, Andrews BJ, Araya MC, Arnold DWD, Biggs J, Cooper C, Cottrell E, Furtney M, Hickey J, Jay J, Lloyd R, Parker AL, Pritchard ME, Robertson E, Venzke E, Williamson JL (2016) Synthesis of global satellite observations of magmatic and volcanic deformation: implications for volcano monitoring & the lateral extent of magmatic domains. *J Appl Volcanol* 7:2. <https://doi.org/10.1186/s13617-018-0071-3>

Elburg MA, Van Bergen MJ, Foden JD (2004) Subducted upper and lower continental crust contributes to magmatism in the collision sector of the Sunda-Banda arc, Indonesia. *Geology* 32: 41-44. doi: 10.1130/G19941.1

Elburg MA, Kamenetsky VS, Foden JD, Sobolev A (2007) The origin of medium-K ankaramitic arc magmas from Lombok (Sunda arc, Indonesia): Mineral and melt inclusion evidence. *Chem Geol* 240: 260-279. doi: 10.1016/j.chemgeo.2007.02.015.

Favalli MM, Karátson D, Mazzuoli R, Pareschi MT, Ventura G (2005) Volcanic geomorphology and tectonics of the Aeolian archipelago (Southern Italy) based on integrated DEM data. *Bull Volcanol* 68: 157-170. <https://doi.org/10.1007/s00445-005-0429-3>

802 Fioletov VE, McLinden CA, Krotkov N, Li C (2015) Lifetimes and emissions of SO₂ from point
803 sources estimated from OMI. *Geophys Res Lett* 42, 1969–1976.
804 <https://doi.org/10.1002/2015GL063148>
805

806 Fioletov VE, McLinden CA, Krotkov N, Li C, Joiner J, Theys N, Carn N, Moran M (2016) A
807 global catalogue of large SO₂ sources and emissions derived from the Ozone Monitoring
808 Instrument. *Atmos Chem Phys* 16: 11497–11519. doi:10.5194/acp-16-11497-2016.
809

810 Flower VJB, Oommen T, Carn SA (2016) Improving global detection of volcanic eruptions using
811 the Ozone Monitoring Instrument (OMI). *Atmos Meas Tech* 9: 5487–5498. Doi:10 5194/amt-9-
812 5487-2016. <https://doi.org/10.5194/amt-9-5487-2016>
813

814 Francalanci L, Tommasini S, Conticelli S, Davies GR (1999) Sr isotope evidence for short magma
815 residence time for the 20th century activity at Stromboli volcano, Italy. *Earth Planet Sci Lett* 167
816 (1-2): 61-69. [https://doi.org/10.1016/S0012-821X\(99\)00013-8](https://doi.org/10.1016/S0012-821X(99)00013-8)
817

818 Francis P, Oppenheimer C, Stevenson D (1993) Endogenous growth of persistently active
819 volcanoes. *Nature* 366: 554-557. doi:10.1038/366554a0
820

821 Ganci G, Vicari A, Cappello A, Del Negro C (2012) An emergent strategy for volcano hazard
822 assessment: from thermal satellite monitoring to lava flow. *Remote Sens Environ* 119:197–207.
823 <http://doi.org/10.1016/j.rse.2011.12.021>
824

825 Gaudin D, Taddeucci J, Scarlato P, del Bello E, Ricci T, Orr T, Houghton B, Harris A, Rao S,
826 Bucci A (2017) Integrating puffing and explosions in a general scheme for Strombolian-style
827 activity. J Geophys Res Solid Earth 122. <https://doi.org/10.1002/2016JB013707>
828

829 Global Volcanism Program (1971) Report on Tinakula (Solomon Islands). CSLP 1301, 87-71. D.
830 Dawea-taukalo, Sub Station, Graciosa Bay, Santa Cruz, B.S.I.P.; R.B. Thompson, Geological
831 Survey Dept., Honiara, Guadalcanal, B.S.I.P.
832 https://volcano.si.edu/volcano.cfm?vn=256010#bgvn_197110
833

834 Global Volcanism Program (2003) Report on Tinakula (Solomon Islands). In: Venzke, E (ed.),
835 Bulletin of the Global Volcanism Network, 28:1. Smithsonian Institution.
836 <http://dx.doi.org/10.5479/si.GVP.BGVN200301-256010>
837

838 Global Volcanism Program (2006) Report on Tinakula (Solomon Islands). In: Wunderman, R
839 (ed.), Bulletin of the Global Volcanism Network, 31:3. Smithsonian Institution.
840 <http://dx.doi.org/10.5479/si.GVP.BGVN200603-256010>
841

842 Global Volcanism Program (2007) Report on Batu Tara (Indonesia). In: Wunderman, R (ed.),
843 Bulletin of the Global Volcanism Network, 32:12. Smithsonian Institution.
844 <http://dx.doi.org/10.5479/si.GVP.BGVN200712-264260>
845

846 Global Volcanism Program (2008) Report on Batu Tara (Indonesia). In: Wunderman, R (ed.),
847 Bulletin of the Global Volcanism Network, 33:7. Smithsonian Institution.
848 <https://dx.doi.org/10.5479/si.GVP.BGVN200807-264260>

849

850 Global Volcanism Program (2011) Report on Batu Tara (Indonesia). In: Wunderman, R (ed.),

851 Bulletin of the Global Volcanism Network, 36:10. Smithsonian Institution.

852 <http://dx.doi.org/10.5479/si.GVP.BGVN201110-264260>

853

854 Global Volcanism Program (2012) Report on Tinakula (Solomon Islands). In: Wunderman, R

855 (ed.), Bulletin of the Global Volcanism Network, 37:6. Smithsonian Institution.

856 <https://dx.doi.org/10.5479/si.GVP.BGVN201206-256010>

857

858 Global Volcanism Program (2013) Volcanoes of the World, v. 4.6.6. Venzke, E (ed.). Smithsonian

859 Institution. Downloaded 14 Mar 2018. <https://dx.doi.org/10.5479/si.GVP.VOTW4-2013>

860

861 Global Volcanism Program (2014) Report on Batu Tara (Indonesia). In: Wunderman, R (ed.),

862 Bulletin of the Global Volcanism Network, 39:1. Smithsonian Institution.

863 <http://dx.doi.org/10.5479/si.GVP.BGVN201401-264260>

864

865 Global Volcanism Program (2016) Report on Batu Tara (Indonesia). In: Venzke, E (ed.), Bulletin

866 of the Global Volcanism Network, 41:11. Smithsonian Institution.

867

868 Global Volcanism Program (2017) Report on Tinakula (Solomon Islands). In: Sennert, S K (ed.),

869 Weekly Volcanic Activity Report, 18 October-24 October 2017. Smithsonian Institution and US

870 Geological Survey.

871

872 Harris AJL (2013) Thermal Remote Sensing of Active Volcanoes. A User's Manual Cambridge
873 University Press, pp. 736. <https://doi.org/10.1017/CBO9781139029346>
874

875 Harris AJL, Stevenson D (1997) Magma budgets and steady-state activity of Vulcano and
876 Stromboli. Geophys Res Lett 24(9): 1043-1046. <https://doi.org/10.1029/97GL00861>
877

878 Harris AJL, Baloga SM (2009) Lava discharge rates from satellite-measured heat flux. Geophys
879 Res Lett 36, L19302. <https://doi.org/10.1029/2009GL039717>
880

881 Harris AJL, Murray JB, Aries SE, Davies MA, Flynn LP, Wooster MJ, Wright R, Rothery D
882 (2000) Effusion rate trends at Etna and Krafla and their implications for eruptive mechanisms. J
883 Volcanol Geotherm Res 102: 237-270.
884

885 Harris AJL, Flynn LP, Keszthelyi L, Mouginis-Mark PJ, Rowland SK, Resing JA (1998)
886 Calculation of lava effusion rates from Landsat TM data. Bull Volcanol 60:52–71.
887

888 Harris AJL, Dehn J, Calvari S (2007) Lava effusion rate definition and measurement: A review.
889 Bull Volcanol 70(1): 1-22. <https://doi.org/10.1007/s00445-007-0120-y>
890

891 Harris AJL, Steffke A, Calvari S, Spampinato L (2011) Thirty years of satellite-derived lava
892 discharge rates at Etna: implications for steady volumetric output. J Geophys Res 116: B08204.
893 <http://dx.doi.org/10.1029/2011JB008237>.
894

895 Harris AJL, Villeneuve N, Di Muro A, Ferrazzini V, Peltier A, Coppola D, Favalli M, Bachèlery
896 P, Froger JL, Gurioli L, Moune S, Vlastélic I, Galle B, Arellano S (2017) Effusive crises at Piton
897 de la Fournaise 2014–2015: a review of a multi-national response model. J Appl Volcanol 6 (11):
898 <https://doi.org/10.1186/s13617-017-0062-9>
899

900 Hayer CS, Wadge G, Edmonds M, Christopher T (2016) Sensitivity of OMI SO₂ measurements
901 to variable eruptive behaviour at Soufrière Hills Volcano, Montserrat. J Volcanol Geotherm Res
902 312:1-10. <https://doi.org/10.1016/j.jvolgeores.2016.01.014>
903

904 Jarvis A, Reuter HI, Nelson A, Guevara E (2008) Hole-filled seamless SRTM data V4,
905 International Centre for Tropical Agriculture (CIAT), available from <http://srtm.csi.cgiar.org>.
906

907 Koeppen WC; Pilger E, Wright R (2011) Time series analysis of infrared satellite data for detecting
908 thermal anomalies: a hybrid approach. Bull Volcanol 73 (5): 577-593. doi:10.1007/s00445-010-
909 0427-y
910

911 Krotkov NA, Li C, Leonard P (2014) OMI/Aura Sulphur Dioxide (SO₂) Total Column Daily L2
912 Global Gridded 0.125 degree x 0.125 degree V3. Greenbelt, MD, USA, Goddard Earth Sciences
913 Data and Information Services Center (GES DISC): Accessed [01032018-10032018]
914 10.5067/Aura/OMI/DATA2023.
915

916 Krueger AJ, Walter LS, Bhartia PK, Schnetzler CC, Krotkov NA, Sprod I, Bluth GJS (1995)
 917 Volcanic sulfur dioxide measurements from the total ozone mapping spectrometer instruments. J
 918 Geophys Res 100(D7):14057-14056. <https://doi.org/10.1029/95JD01222>
 919
 920 Landi P, Corsaro RA, Francalanci L, Civetta L, Miraglia L, Pompilio M, Tesoro R (2009) Magma
 921 during the 2007 Stromboli eruption (Aeolian Islands, Italy): mineralogical, geochemical and
 922 isotopic data. J Volcanol Geotherm Res 182 (3-4): 255–268.
 923
 924 Li C, Krotkov NA, Carn SA, Zhang Y, Spurr RJD, Joiner J (2017). New-generation NASA Aura
 925 Ozone Monitoring Instrument volcanic SO₂ dataset: Algorithm description, initial results, and
 926 continuation with the Suomi-NPP Ozone Mapping and Profiler Suite. Atmos. Meas. Tech. 10:
 927 445-458. doi:10.5194/amt-10-445-2017
 928
 929 Machado F (1974) The search for magmatic reservoirs. In: Civetta L, Gasparini P, Luongo G,
 930 Rapolla A (ed), Physical Volcanology, Elsevier, Amsterdam, pp.255-273.
 931
 932 Marani MP, Gamberi F, Rosi M, Bertagnini A, Di Roberto A (2009) Subaqueous density flow
 933 processes and deposits of an island volcano landslide (Stromboli Island, Italy). Sedimentology 56:
 934 1488–1504. <https://doi.org/10.1111/j.1365-3091.2008.01043.x>
 935
 936 Mastin LG, Lisowski M, Roeloffs E, Beeler N (2008) Improved constraints on the estimated size
 937 and volatile content of the Mount St. Helens magma system from the 2004–2008 history of dome
 938 growth and deformation. Geophys Res Lett 36: L20304. <https://doi.org/10.1029/2009GL039863>

939

940 McCormick-Kilbride B, Edmonds M, Biggs J, (2016) Observing eruptions of gas-rich,
941 compressible magmas from space. Nat Comm 7: 13744. Doi:10.1038/ncomms13744

942

943 Métrich N. Bertagnini A, Di Muro A (2009) Conditions of magma storage, degassing and ascent
944 at Stromboli: New insights into the volcano plumbing system with inferences on the eruptive
945 dynamics. J Petrol 51 (3): 603-626. doi: 10.1093/petrology/egp083.

946

947 Murphy SW, Wright R, Oppenheimer C, Filho CRS (2013) MODIS and ASTER synergy for
948 characterizing thermal volcanic activity. Remote Sens Environ 131:195–205.
949 <http://dx.doi.org/10.1016/j.rse.2012.12.005>

950

951 NDMO Report 2017 National Disaster Management Office, Solomon Islands, Report No. 2
952 Tinakula Volcano, 2017.10.26. [http://www.ndmo.gov.sb/index.php/situation-report/197-national-](http://www.ndmo.gov.sb/index.php/situation-report/197-national-situation-report-02-tinakula-volcano)
953 [situation-report-02-tinakula-volcano](http://www.ndmo.gov.sb/index.php/situation-report/197-national-situation-report-02-tinakula-volcano)

954

955 Newhall CG, Self S (1982) The volcanic explosivity index (VEI): an estimate of explosive
956 magnitude for historical volcanism. J Geophys Res 87 (C2): 1231-1238.

957

958 Oppenheimer C, McGonigle AJS, Allard P, Wooster MJ, Tsanev V (2004) Sulfur, heat, and
959 magma budget of Erta ‘Ale lava lake, Ethiopia. Geology 32 (6): 509–512. doi: 10.1130/G20281.1

960

961 Parfitt EA, Wilson L, (1995) Explosive volcanic eruptions-IX. The transition between Hawaiian-
 962 style lava fountaining and Strombolian explosive activity. *Geophys J Int* 121(1): 226–232.
 963 <https://doi.org/10.1111/j.1365-246X.1995.tb03523.x>
 964

965 Pieri D, Abrams M (2004) ASTER watches the world’s volcanoes: a new paradigm for
 966 volcanological observations from orbit. *J Volcanol Geotherm Res* 135: 13–28.
 967 <https://doi.org/10.1016/j.jvolgeores.2003.12.018>
 968

969 Pistolesi M, Delle Donne D, Pioli L, Rosi M, Ripepe M (2011) The 15 March 2007 explosive crisis
 970 at Stromboli volcano, Italy: assessing physical parameters through a multidisciplinary approach. *J*
 971 *Geophys Res*, 116, B12206. <https://doi.org/10.1029/2011JB008527>
 972

973 Pyle DM, Mather TA, Biggs J (2013) Remote sensing of volcanoes and volcanic processes:
 974 integrating observation and modelling – introduction. In: Pyle, D. M., Mather, T. A. & Biggs, J.
 975 (ed), *Remote Sensing of Volcanoes and Volcanic Processes: Integrating Observation and*
 976 *Modelling*. Geological Society, London, Sp Pub 380, pp. 1-13. doi:
 977 <https://doi.org/10.1144/SP380.14>
 978

979 Ramsey MS (2016) Synergistic use of satellite thermal detection and science: a decadal perspective
 980 using ASTER. In: Harris AJL, De Groeve T, Garel F, Carn SA (ed), *Detecting, Modelling, and*
 981 *Responding to Effusive Eruptions*, Geological Society, London, Sp Pub 426: 115-136.
 982 <https://doi.org/10.1144/SP426.23>
 983

984 Ramsey MS, Harris AJL (2013) Volcanology 2020: how will thermal remote sensing of volcanic
 985 surface activity evolve over the next decade? J Volcanol Geotherm Res 249: 217–233.
 986 <https://doi.org/10.1016/j.jvolgeores.2012.05.011>
 987
 988 Reath KA, Ramsey MS, Dehn J, Webley PW (2016) Predicting eruptions from precursory activity
 989 using remote sensing data hybridization. J Volcanol Geotherm Res 321: 18-30.
 990 <https://doi.org/10.1016/j.jvolgeores.2016.04.027>
 991
 992 Ripepe M, Delle Donne D, Harris A, Marchetti E, Ulivieri G (2008) Dynamics of Stromboli
 993 activity. In: Calvari S, Inguaggiato S, Puglisi G, Ripepe M, Rosi M (ed), Learning from Stromboli:
 994 AGU Geophysics Monograph Series, 182, Washington DC, pp. 39–48.
 995
 996 Ripepe M, Delle Donne D, Genco R, Maggio G, Pistolesi M, Marchetti E, Lacanna G, Ulivieri G,
 997 Poggi P (2015) Volcano seismicity and ground deformation unveil the gravity-driven magma
 998 discharge dynamics of a volcanic eruption. Nature Commun 6: 6998. doi:10 1038/ncomms7998.
 999
 1000 Ripepe M, Pistolesi M, Coppola D, Delle Donne D, Genco R, Lacanna G, Laiolo M, Marchetti E,
 1001 Ulivieri G, Valade S (2017) Forecasting Effusive Dynamics and decompression rates by
 1002 magmastatic model at Open-vent Volcanoes. Sci Rep 7: 3885. [10.1038/s41598-017-03833-3](https://doi.org/10.1038/s41598-017-03833-3)
 1003
 1004 Rosi M, Bertagnini A, Landi P (2000) Onset of persisting activity at Stromboli Volcano (Italy).
 1005 Bull Volcanol 62: 294-300. <https://doi.org/10.1007/s004450000098>
 1006

1007 Rosi M, Pistolesi M, Bertagnini A, Landi P, Pompilio M, Di Roberto A (2013) Stromboli volcano,
 1008 Aeolian Islands (Italy): present eruptive activity and hazards. In: Lucchi F, Peccerillo A, Keller J,
 1009 Tranne CA, Rossi PL (ed) The Aeolian Islands Volcanoes, Geological Society London Memoirs
 1010 37(1), chapter 14, The Geological Society of London, pp.473-490. <https://doi.org/10.1144/M37>
 1011 14. <https://doi.org/10.1144/M37.14>
 1012
 1013 Rothery D, Coppola D, Saunders C (2005) Analysis of volcanic activity patterns using MODIS
 1014 thermal alerts. Bull Volcanol 67 (6): 539–556. <https://doi.org/10.1007/s00445-004-0393-3>
 1015
 1016 Scandone R (1979) Effusion rate and energy balance of Parícutín eruption (1943-1952),
 1017 Michoacán, Mexico. J Volcanol Geotherm Res 6: 49-59.
 1018
 1019 Rowland SK, Harris AJL, Wooster MJ, Garbeil H, Mouginis-Mark PJ, Amelung F, Wilson L
 1020 (2003) Volumetric characteristics of lava flows from interferometric radar and multispectral
 1021 satellite data: the 1995 Fernandina and 1998 Cerro Azul eruptions in the western Galápagos. Bull
 1022 Volcanol 65:311-330.
 1023
 1024 Scandone R (1996) Factors controlling the temporal evolution of explosive eruptions. J Volcanol
 1025 Geotherm Res 72 (1-2): 71-83. [https://doi.org/10.1016/0377-0273\(95\)00086-0](https://doi.org/10.1016/0377-0273(95)00086-0)
 1026
 1027 Schuth S, Münker C, König S, Qopoto C, Basi S, Garbe-Schönberg D, Ballhaus C (2009)
 1028 Petrogenesis of Lavas along the Solomon Island Arc, SW Pacific: Coupling of Compositional
 1029 Variations and Subduction Zone Geometry. J Petrol 50 (5): 781-811.
 1030 <https://doi.org/10.1093/petrology/egp019>

1031

1032 Shinohara H (2008) Excess degassing from volcanoes and its role on eruptive and intrusive

1033 activity. *Review of Geophysics* 46(4): RG4005. <https://doi.org/10.1029/2007RG000244>

1034

1035 Spera F (1984) Some numerical experiments on the withdrawal of magma from crustal reservoirs.

1036 *J Geophys Res* 89: 8222–8236.

1037

1038 Stasiuk MV, Jaupart C, Sparks RSJ (1993) Influence of cooling on lava-flow dynamics. *Geology*

1039 21: 335–338

1040

1041 Steffke AM, Harris AJL, Burton M, Caltabiano T, Salerno GG (2011) Coupled use of COSPEC

1042 and satellite measurements to define the volumetric balance during effusive eruptions at Mt. Etna,

1043 Italy. *J Volcanol Geotherm Res* 205 (1-2): 47-53, doi: 10.1016/j.jvolgeores.2010.06.004

1044

1045 Theys N, Campion R, Clarisse L, Brenot H, van Gent J, Dils B, Corradini S, Merucci L, Coheur

1046 P-F, Van Roozendaal M, Hurtmans D, Clerbaux C, Tait S, Ferrucci F (2013) Volcanic SO₂ fluxes

1047 derived from satellite data: a survey using OMI, GOME-2, IASI and MODIS. *Atmos Chem Phys*

1048 13: 5945–5968. <https://doi.org/10.5194/acp-13-5945-2013>

1049

1050 Valade S, Lacanna G, Coppola D, Laiolo M, Pistolesi M, Delle Donne D, Genco R, Marchetti E,

1051 Ulivieri G, Allocca C, Cigolini C, Nishimura T, Poggi P, Ripepe M (2016) Tracking dynamics of

1052 magma migration in open-conduit systems. *Bull Volcanol* 78 (11). [https://doi.org/10.1007/s00445-](https://doi.org/10.1007/s00445-016-1072-x)

1053 [016-1072-x](https://doi.org/10.1007/s00445-016-1072-x)

1054

1055 Van Bergen MJ, Vroon PZ, Varekamp JC, Poorter RPE (1992) The origin of the potassic rock
 1056 suite from Batu Tara volcano (East Sunda Arc, Indonesia). *Lithos* 28 (3-6): 261-282.
 1057 [https://doi.org/10.1016/0024-4937\(92\)90010-V](https://doi.org/10.1016/0024-4937(92)90010-V)

1058

1059 Vaughan RG, Keszthelyi LP, Lowenstern JB, Jaworowski C, Heasler H (2012) Use of ASTER
 1060 and MODIS thermal infrared data to quantify heat flow and hydrothermal change at Yellowstone
 1061 National Park. *J Volcanol Geotherm Res* 233–234: 72-89.
 1062 <https://doi.org/10.1016/j.jvolgeores.2012.04.022>.

1063

1064 Ventura G (2013) Kinematics of the Aeolian volcanism (Southern Tyrrhenian sea) from
 1065 geophysical and geological data. In: Lucchi F, Peccerillo A, Keller J, Tranne CA, Rossi PL (eds.)
 1066 The Aeolian Islands Volcanoes, Geological Society London Memoirs 37(1), chapter 2, The
 1067 Geological Society of London, pp.3-11. <https://doi.org/10.1144/M37.2>

1068

1069 Wadge G (1981) The variation of magma discharge during basaltic eruptions. *J Volcanol*
 1070 *Geotherm Res* 11(2-4): 139-168. [https://doi.org/10.1016/0377-0273\(81\)90020-2](https://doi.org/10.1016/0377-0273(81)90020-2)

1071

1072 Wooster MJ, Zhukov B, Oertel D (2003) Fire radiative energy for quantitative study of biomass
 1073 burning: derivation from the BIRD experimental satellite and comparison to MODIS fire products.
 1074 *Remote Sens Environ* 86: 83–107. [https://doi.org/10.1016/S0034-4257\(03\)00070-1](https://doi.org/10.1016/S0034-4257(03)00070-1)

1075

1076 Wright R, Carn SA, Flynn LP (2005) A satellite chronology of the May–June 2003 eruption of
1077 Anatahan volcano. *J Volcanol Geotherm Res* 146(1-3), 102-116. doi:
1078 <https://doi.org/10.1016/j.jvolgeores.2004.10.021>
1079
1080 Wright R, Blackett M, Hill-Butler C (2015) Some observations regarding the thermal flux from
1081 Earth's erupting volcanoes for the period of 2000 to 2014. *Geophys Res Lett* 42:282–289.
1082 <https://doi.org/10.1002/2014GL061997>
1083
1084 Zakšek K, Hort M, Lorenz E (2015) Satellite and Ground Based Thermal Observation of the 2014
1085 Effusive Eruption at Stromboli Volcano. *Remote Sensing* 7: 17190–17211. doi:
1086 10.3390/rs71215876.
1087
1088
1089
1090
1091
1092
1093
1094
1095
1096
1097
1098

Table 1. Summary of the main features characterising Stromboli, Batu Tara and Tinakula volcanoes.

		Stromboli	Batu Tara	Tinakula
Tectonic Setting		Rifting process developing within an arc collision zone ^a	Subduction related island-arc ^b	Subduction related island-arc ^c
Morphology	Total Height (m)	~3000 ^d	~2500 - 3000 ^e	~3000 - 4000 ^f
	Elevation (m a.s.l.)	924 ^d	748	851
	Area (subaerial, km ²)	12.6 ^d	~5.2	~7.8
	Volume (subaerial, km ³)	~3.88	~1.3	~2.2
	Mean Slope	~25 %	~22 %	~24 %
	Flank collapse sector Slope	~36 %	~32 %	~36 %
Volcanic Activity	Effusive	Flank eruptions ^g - Summit overflows ^h	Lava flows (e.g., April 2007) ⁱ	Fissure eruption - Summit overflows (e.g., Sept. 1971 - May 2012) ^{j,k}
	Type	Intermittent mild Strombolian explosions; rare Vulcanian paroxysms ^l	Strombolian and Vulcanian explosions ^m	Strombolian and Vulcanian explosions ^{n,o}
	Max Plume Altitude (m)	~3000 m (e.g., 5 April 2003) ^p	~3700 (e.g., Jul 2008) ^q	~10700 (e.g., 21 Oct 2017) ^o
	Max VEI	VEI = 1-2 (e.g., 5 April 2003) ^l	VEI = 2 (e.g., Jul 2008) ^q	VEI = 3 (e.g., 21 Oct. 2017) ^r
	Persistent Degassing	SO ₂ flux 150–200 t/d ^s 30 December 2002; Mass	- (?)	- (?)
	Volcanogenic tsunamis	failure events (volumes 25–30 × 10 ⁶ m ³) ^t	- (?)	06 September 1971 ^j
Products	Type	Scoria bombs, lithic blocks, ash, lavas, “golden pumices”, pyroclastic flows ¹	Scoria bombs, ash, lavas, small pyroclastic flows ^u	Scoria bombs, ash and lavas ^k
	Composition (SiO ₂)	Basalts - Basaltic Andesites (49-51 wt%*) ^v	Basanites - Tephrites (45-54 wt%*) ^e	Basalts (49-50 wt%*) ^c
	Geochemistry	Calc-Alkaline, High-K Calc-Alkaline, Shoshonitic, Potassic ^w	Potassic-Ultrapotassic ^e	Calc-Alkaline ^c

In *italics* data retrieved from Google Earth Images; * identify SiO₂ of the 2007-2014 lavas of Stromboli

a - Ventura (2013); b - Elburg et al. (2004); c - Schuth et al. (2004); d - Favalli et al. (2005); e - Van Bergen et al. (1992); f - Davies et al. (1986); g - Barberi et al. (1993); h - Calvari et al. (2014);

i - GVP (1971); j - GVP (2012); k - Rosi et al. (2013); l - GVP (2014); m - GVP (2003); n - GVP (2017); o - GVP (2008); p - Pistolesi et al. (2011); q - GVP (2008); r - GVP (2017); s - Burton et al. (2009);

t - Marani et al. (2009); u - GVP (2016); v - Landi et al. (2009); w - Francalanci et al. (1999).

Table 1. Summary of the main features characterising Stromboli, Batu Tara and Tinakula volcanoes, with data in *italics* retrieved from Google Earth Images.

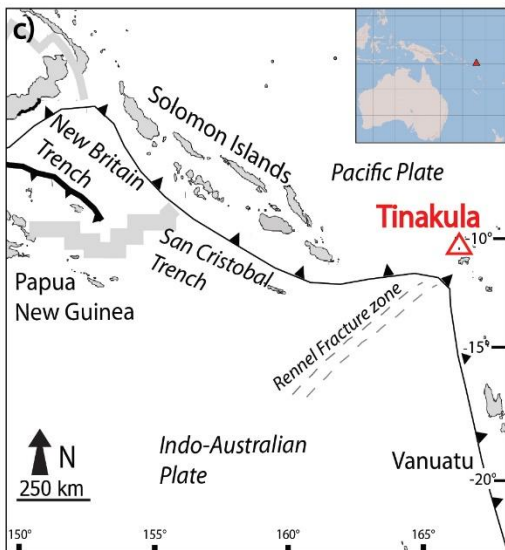


Fig. 1 Simplified tectonic setting of the areas of (a) Stromboli, (b) Batu Tara and (c) Tinakula, after Ventura (2013), Elburg et al. (2007) and Davies et al. (2005), respectively. The insets indicate the world geographical position of the volcanoes.

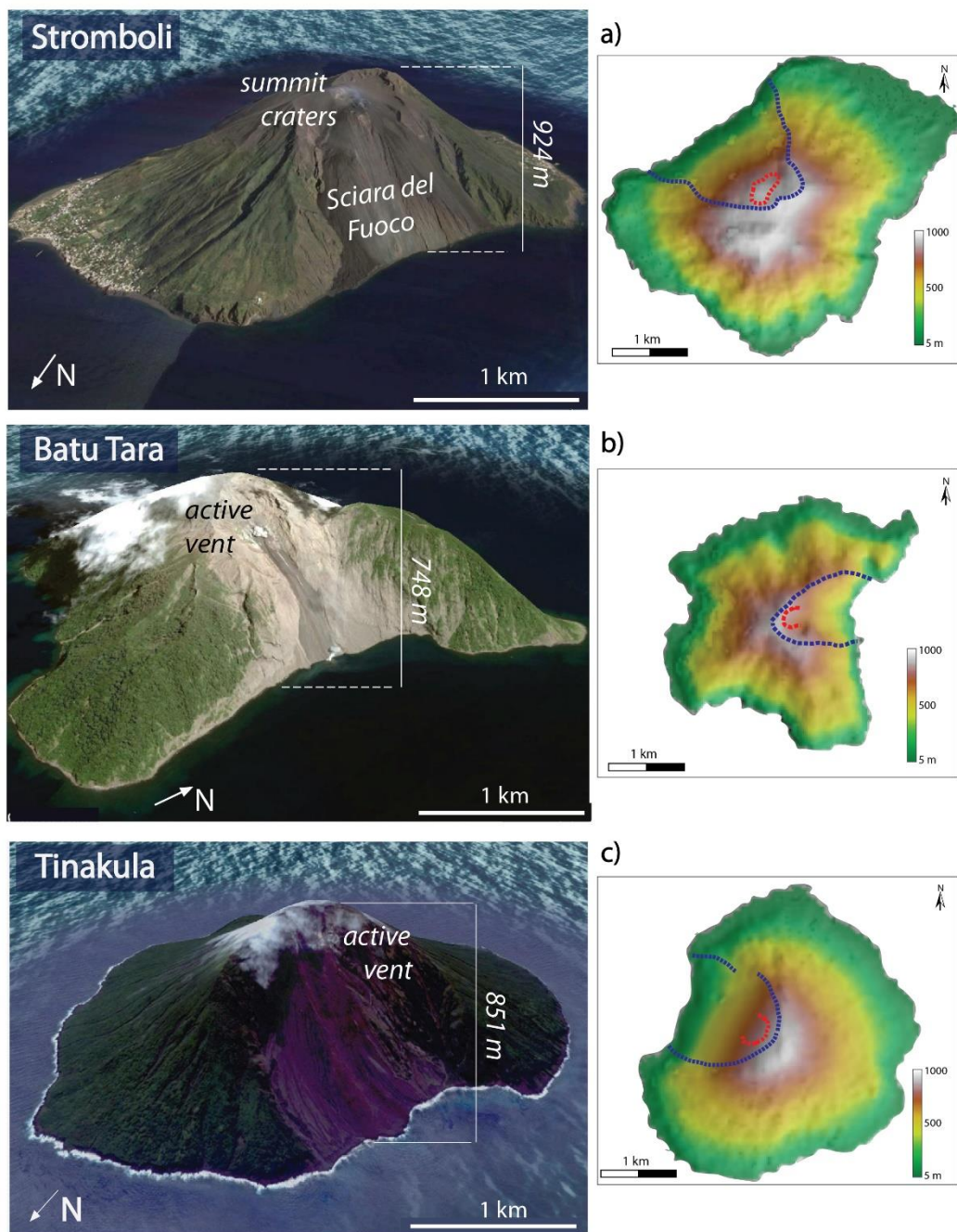


Fig. 2 Google Earth views with elevation (meters above sea level) and crater(s) position, and associated 90-meter Digital Elevation Models (DEM) of the islands. Red lines denote the crater areas, and blue lines show the boundaries of flank scarps. Google Earth Images © Google and DigitalGlobe. DEMs derive from the NASA Shuttle Radar Topographic Mission (SRTM) database (Jarvis et al. 2008); products are freely available and downloadable by CGIAR-CSI, <http://srtm.csi.cgiar.org>.

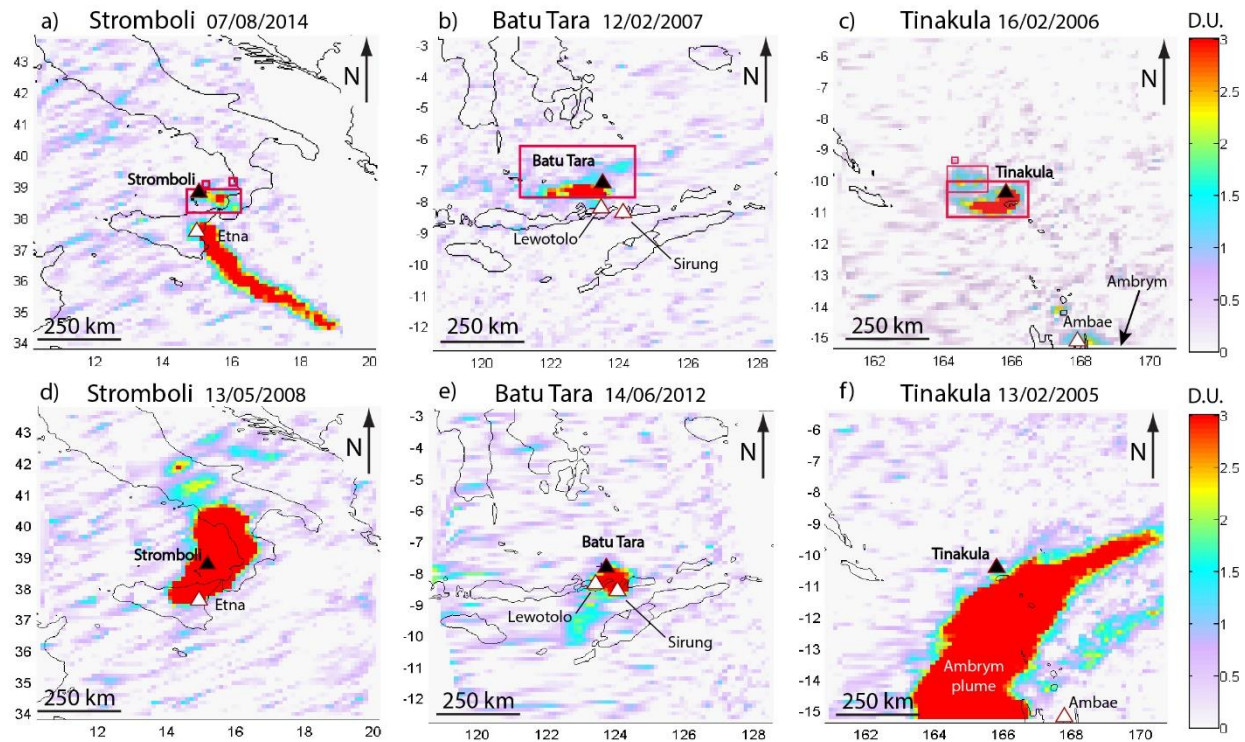


Fig. 3 Examples of SO₂ density maps at PBL layer (see Method Section) processed for Stromboli (a-d), Batu Tara (b-e) and Tinakula (c-f). Maps are centred on volcanoes and cover an area of 10° × 10°. Magenta rectangles (in a-b-c) represent the cluster(s) identified by the detection algorithm. The images d-e-f represent days where plumes belonging from adjacent volcanic sources (white triangles) contaminated the atmosphere of the target volcanoes (black triangles).

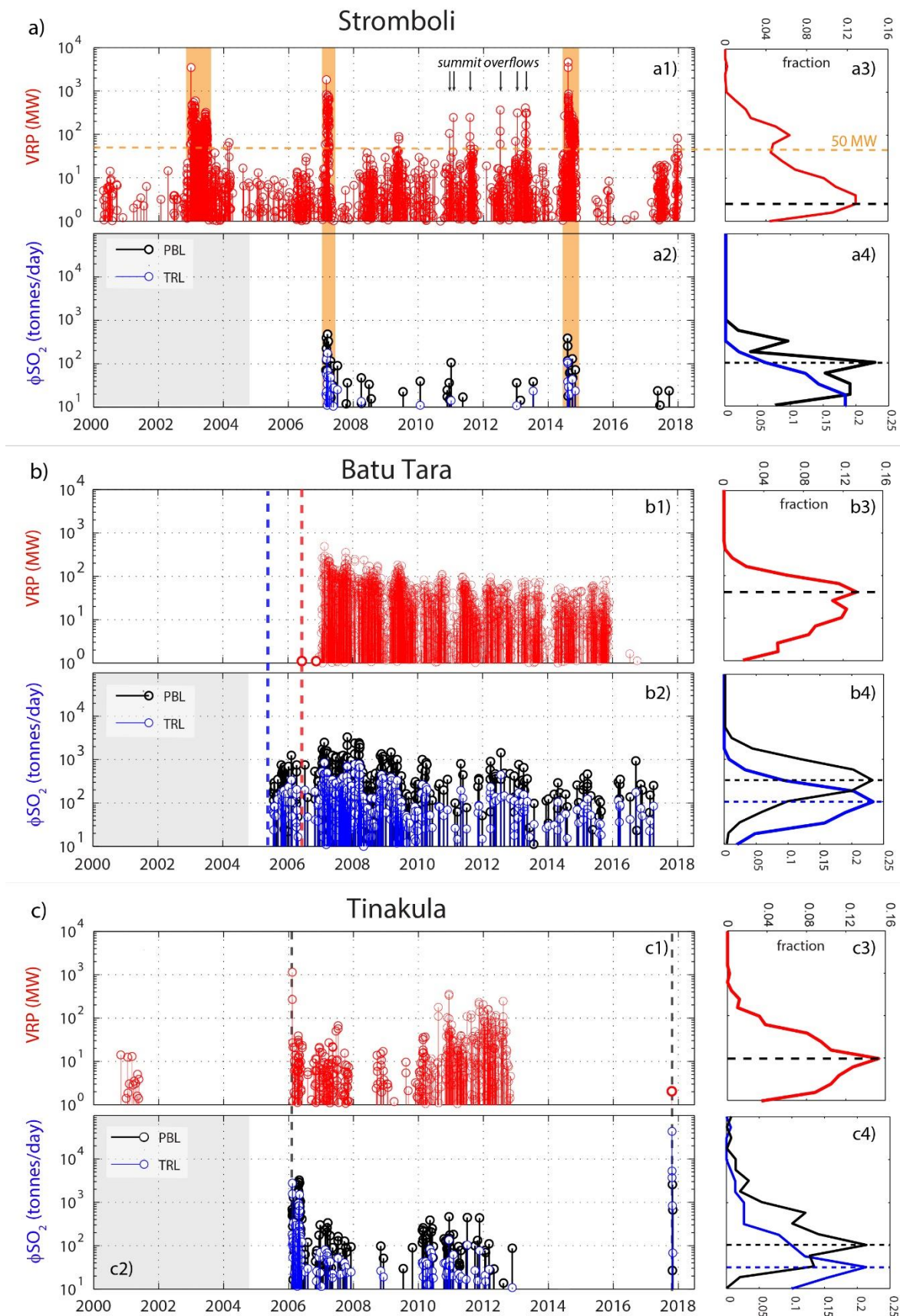


Fig. 4#1-2 2000-2017 VRP and ϕSO_2 (on a logarithmic scale) time-series retrieved by processing MODIS images and OMSO2 Level2G data, at Stromboli (a), Batu Tara (b) and Tinakula (c). In (a), pale orange fields and minor black arrows represent, respectively, the main effusive phase and overflows episodes, while the horizontal orange dotted line marks the transition from strombolian to effusive regimes as indicated by Coppola et al. (2012). In (b), red and blue dotted lines mark the first detection on VRP and ϕSO_2 , respectively. In (c), main episodes of the 11 February 2006 and 21 October 2017 have been reported with black dotted lines. #3-4) represent the distribution of the log-scale values for VRP (#3) and ϕSO_2 (#4). Blue and black lines show the ϕSO_2 values at TRL and PBL levels, respectively; dotted lines mark the modal peak.

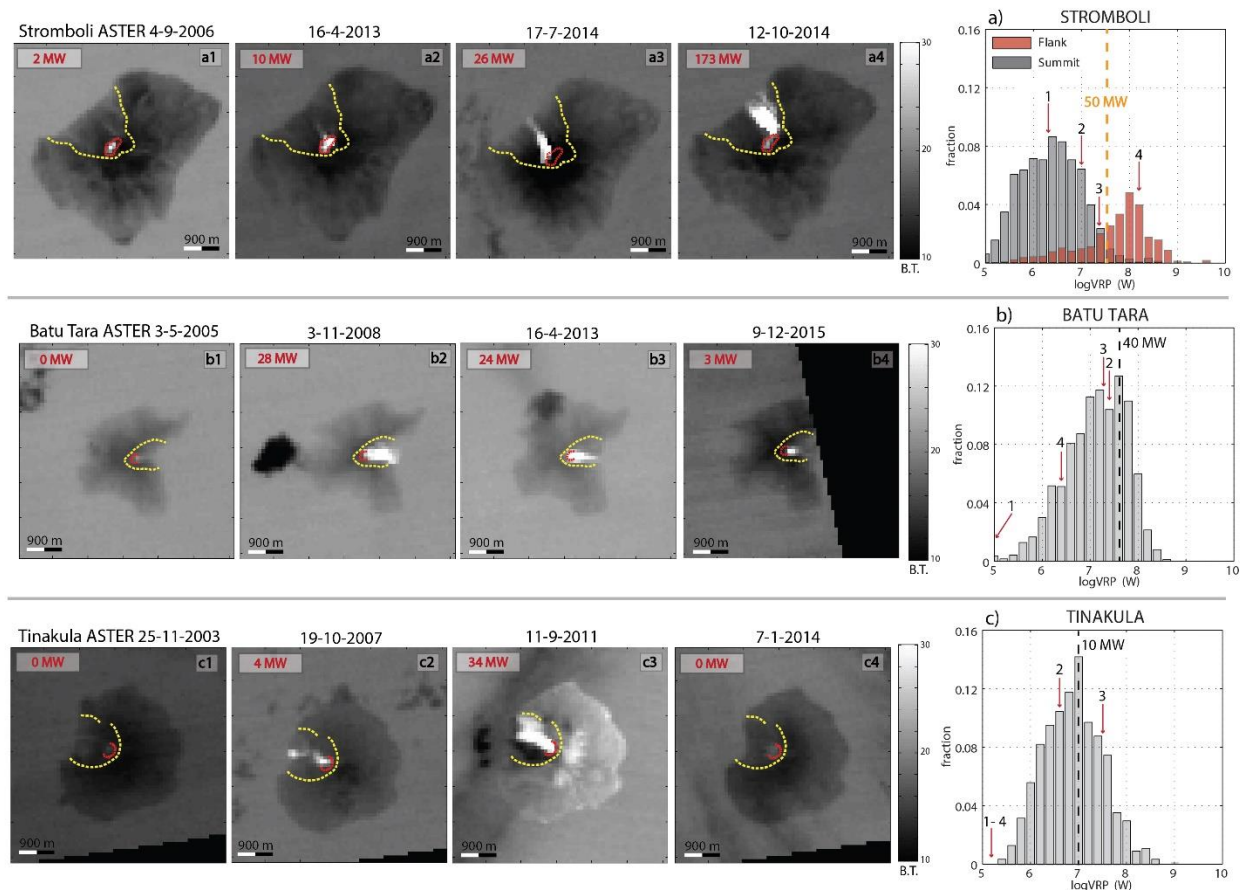


Fig. 5 Histograms of the log-VRP data of the three volcanoes. The separation on flank and summit eruption at Stromboli has been obtained by using already reported lava flow duration (see Ripepe et al. 2017). The orange dotted line marks the transition from strombolian to effusive regimes at Stromboli; the black dotted lines mark the modal peak for Batu Tara and Tinakula; the red arrows indicate the four VRP-MODIS measurements corresponding to the selected ASTER images. ASTER images are shown in greyscale, with Brightness Temperature in the Band 13 (TIR region, 10.25–10.95 μm); MW values in red represent the corresponding MODIS heat flux measurement in the same ASTER acquisition (both sensors on Terra satellite). Red line marks the crater areas; yellow dotted line marks the boundaries of flank scarps.

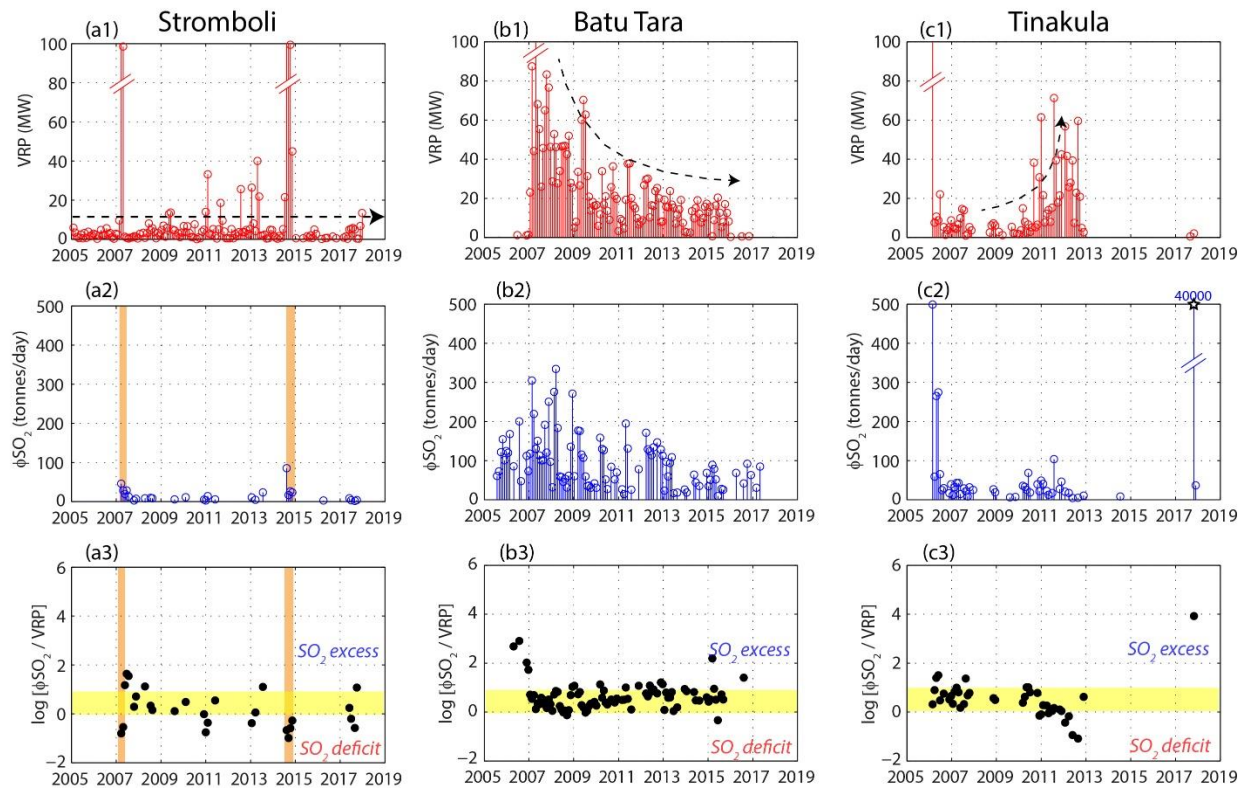


Fig. 6 Time-series of the VRP (#1), ϕSO_2 (#2) and $\phi\text{SO}_2/\text{VRP}$ (#3) for (a#) Stromboli, (b#) Batu Tara and (c#) Tinakula volcanoes. The orange field in (a2, 3) mark the effusive episodes. The

black star in (c2) represent the VEI 3 explosion of 21 October 2017. The black dashed line in (#1) outlines the eruptive trend discussed in the text. The yellow band in (#3) indicates the balanced range whereby the magma supply rate (sourcing the ϕSO_2) and the magma output rate (sourcing the VRP) are equal: eruptions above or below this band may be considered as gas-rich or gas-poor, respectively.

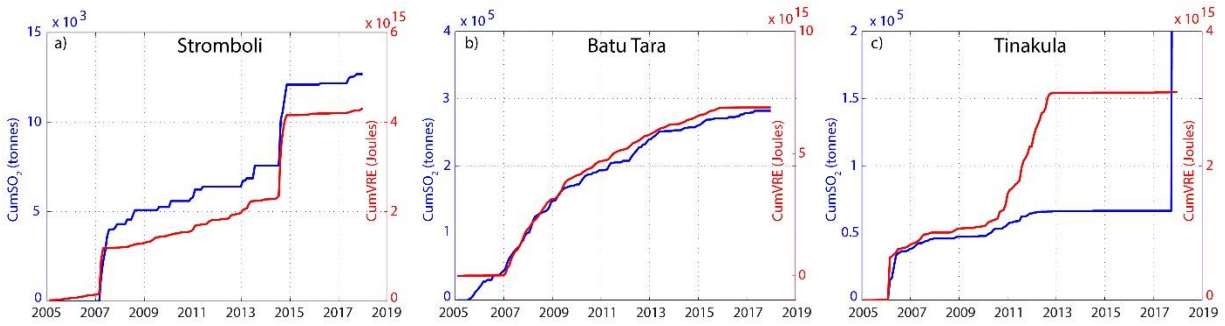


Fig. 7 Cumulative thermal (CumVRE in Joules) and degassing (CumSO₂ in tonnes) emissions recorded between 2005 and 2017 at (a) Stromboli, (b) BatuTara and (c) Tinakula.

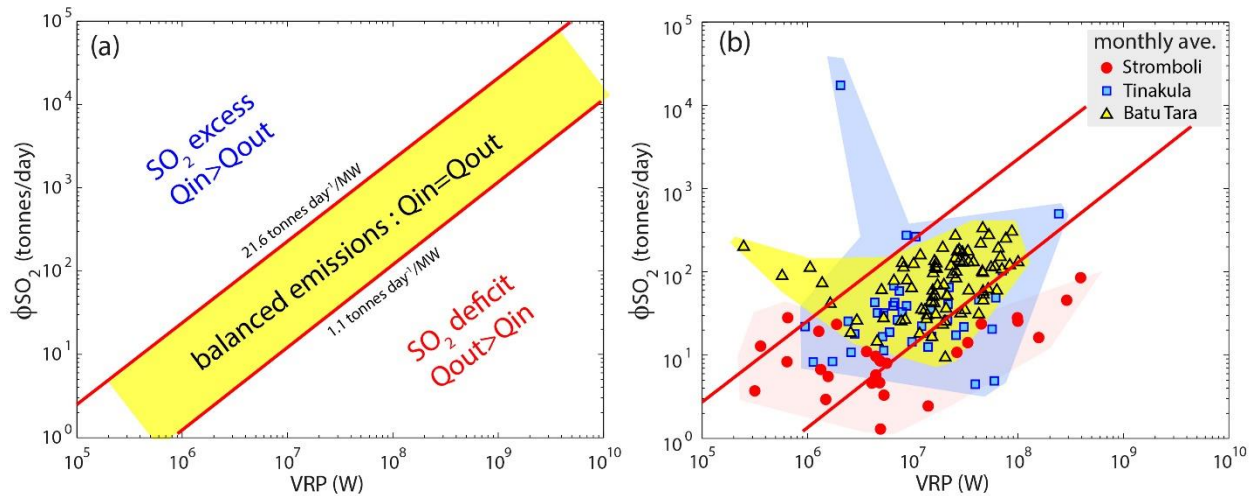


Fig. 8 (a) Schematic plot showing the ϕSO_2 /VRP ratio for degassed/erupted magma budget. The yellow field (equation 3) describes the region of balanced emissions, whereby the the ϕSO_2 and

1166 the VRP are consistent with the eruption of all the degassed magma ($Q_{in} = Q_{out}$). Emission ratios
1167 plotting outside the balanced region indicate a gas-rich (upper left) or gas-poor (lower right)
1168 eruption. **(b)** Monthly mean emissions for the volcanos on the ϕSO_2 /VRP framework. The red lines
1169 limit the balanced region. Shaded coloured fields perimeter the emission ratios for each volcano.
1170 Note how the highly energetic Stromboli's dataset (associated to flank eruptions) falls in the field
1171 of gas-poor eruption, while the single data point of Tinakula VEI 3 eruption of October 2017 falls
1172 in the gas-rich field.